Lattice Symmetry Breaking Perturbation for Spiral Waves

Laurent Charette

Thesis submitted to the Faculty of Graduate and Postdoctoral Studies
in partial fulfillment of the requirements for the degree of Master of Science in
Mathematics [1]

Department of Mathematics and Statistics
Faculty of Science
University of Ottawa

[1]The M.Sc. program is a joint program with Carleton University, administered by the Ottawa-Carleton Institute of Mathematics and Statistics

Abstract

Spiral waves occur in several natural phenomena, including reaction fronts in two-dimension excitable media. In this thesis we attempt to characterize the motion of the spiral tip of a rigidly rotating wave and a linearly travelling wave in the context of a lattice perturbation. This system can be reduced to its center manifold, which allows us to describe the system as ordinary differential equations. This in turn means dynamical systems methods are appropriate to describe the motion of the tip. It is in such a context that we work on spiral waves. We study perturbed rotating waves and travelling waves using standard techniques from dynamical systems theory.

Résumé

Les ondes spiralées se produisent lors de plusieurs phénomènes naturels, dont les fronts de réaction dans les milieux excitables en deux dimensions. Dans cette thèse, nous essayons de caractériser le mouvement de l'extrémité de la spirale en rotation et la spirale en translation, toutes deux soumises à une perturbation en treillis. Le système peut être réduit sur sa variété centrale, ce qui nous permet d'étudier le système par l'entremise d'équations différentielles ordinaires. Ceci signifie que les méthodes de systèmes dynamiques sont adéquates pour décrire le mouvement de l'extrémité. Nous étudions les ondes perturbées en rotation et en translation avec l'aide de techniques standards issues de la théorie des systèmes dynamiques.

Acknowledgements

I would first thank Dr. Victor LeBlanc for thoroughy supervising my work. Many thanks to the Ontario Graduate Scholarship Program (OGS) and to the Natural Sciences and Engineering Research Council of Canada (NSERC) for financial support. For their support, my family also deserves acknowledgemts. Last, but not least, I thank Dr. Monica Nevins for introducing me to a academic career in mathematics and for mentoring me during summer projects.

Dedication

To my great-uncle Gilles, whose dedication to science influenced me greatly.

Contents

List of Figures

List of Tables

Chapter 1

Introduction

The spiral is a shape that is found throughout the natural world; from objects as small as seashells to the massive galaxies like the Milky Way. They are found in fractal patterns and can even be used to solve light diffraction problems [10]. The type of spiral of interest in this thesis is the spiral wave. These waves exhibit oscillatory behaviour on a spiral-shaped front which appears to rotate about a fixed point. This rotation gives the impression that the wavefront flows outward, as pictured in figure 1.1. Spiral waves have been observed in many different systems including Belousov-Zhabotinsky reactions and on electrophysiological tissue. In the latter case, these waves are usually by-products of pathologies, as stated by Keener and Sneyd in Mathematical Physiology [11],"spirals on the heart are fatal, spirals on the cerebral cortex may lead to epileptic seizures, and spirals on the retina may cause hallucinations", therefore a better comprehension of spiral waves is well justified.

The pioneer work that put spiral waves on the workbench of many a mathematician was done by Arthur T. Winfree. He conducted several experiments showcasing spiral waves or its three-dimensional acolyte the scroll wave. For example, in the experiment described in [22], he observed on a petri dish wave patterns in a Belousov-Zhabotinsky reaction. The shape of the patterns were either spiral or of

closed rings. In either case, they were emanating from a source and not necessarily in a circular fashion. He then interpreted this as a section of a scroll wave, which is a three-dimensional system with a section in the shape of a spiral wave and a height.

The presence of spiral waves in excitable media motivated the research of mathematicians. Indeed chemical reactions such as the ones studied by Winfree are governed by the reaction-diffusion equation:

$$\frac{\partial u}{\partial t}(x, y, t) = D\nabla^2 u(x, y, t) + \mathcal{F}(u(x, y, t), \lambda) \tag{1.0.1}$$

where u is an n-dimensional vector function of space coordinates x, y and time t, D is a $n \times n$ diagonal matrix of positive coefficients, ∇^2 is the Laplacian differential operator, λ is a vector in $\mathbb{R}^s$ of arbitrary parameters and $\mathcal{F}$ is an arbitrary function from $\mathbb{R}^{n+s}$ to $\mathbb{R}^n$. This allowed Barkley [2] to conceive a computer model of spiral waves. It was then found in [3] that the periodic circular motion of the wave can undergo a Hopf bifurcation to become a quasi-periodic meandering rotating wave. In the purely rotating case, the circular trajectory means that the system is in a relative equilibrium. That is, in a corotating frame, the wave is static. With the meandering wave, however, observation in a corotating frame gives a periodic orbit. The result in the laboratory frame is an epicycle curve that looks like a flower, with petals (see figure 1.2). It is a curve similar to the trajectory of the moon in orbit around the earth, which itself rotates around the sun. This Hopf bifurcation was naturally associated to a pair of complex-conjugate eigenvalues that crosses the imaginary axis. It was then found that as parameters were changed in order to produce the crossing, the radius of the general motion of the wave in both the rigidly rotating and meandering case got bigger and bigger, until they become travelling waves and their motion becomes unbounded. A further change saw the system return to its former epicycle motion, only to have its "petality" reversed. In a bifurcation diagram, this is shown as a region where meandering happens and a line that marks the inversion of petality. Figure 1.2 gives a coarse overview of the diagram along with approximations of trajectories for

each region. The region where we observe meandering is in light blue and the axes in the figure represent two parameters of the reaction-diffusion equation.

This was analyzed more in depth in [4]. In particular, the inclusion of symmetry to the analysis helped to explain its behaviour. The reaction-diffusion system associated to spiral waves is symmetric with respect to the action of the group $\mathbf{SE}(2)$, the group of all special Euclidian transformations: translations and rotations. Indeed, if you translate or rotate the initial conditions of the system, the result should be the same, only centered in another point and in another orientation. This symmetry coupled with the bifurcation forces five eigenvalues to be on the imaginary axis (three from the symmetries and two from the Hopf bifurcation), which in turn suggested a center-reduction of the system (1.0.1) into an ad hoc five-dimensional system of ordinary differential equations:

$$\begin{aligned}\dot{p} &= F^p(p, \varphi, q)\\ \dot{\varphi} &= F^\varphi(p, \varphi, q)\\ \dot{q} &= F^q(p, \varphi, q),\end{aligned}$$

where $(p, \varphi) \in \mathbb{C} \times \mathbf{S}^1$ correspond to the $\mathbf{SE}(2)$-symmetry and $q \in \mathbb{C}$ corresponds to the Hopf bifurcation.

A rigorous mathematical justification of such a reduction proved to be non-trivial. The group $\mathbf{SE}(2)$ is unbounded and therefore not compact and its action on function spaces such as $C(\mathbb{R}^2, \mathbb{R})$, the space of continuous functions from $\mathbb{R}^2$ to $\mathbb{R}$, is not continuous. For example take the function $f(x, y) = \cos(x) \in C(\mathbb{R}^2, \mathbb{R})$ and apply a rotation. Then it is obvious that even the slightest rotation generates a considerable difference at some point in the function therefore the action is not continuous. It then took the efforts of Sandstede, Scheel, Wulff [20, 21] and of Golubitsky, LeBlanc, Melbourne [8] to bridge that technical gap. The groundwork was then established to use dynamical systems methods to study spiral waves. In fact, it was determined in [8] that the most general set of equations that preserve full Euclidian symmetry on

the center manifold $\mathbb{C} \times \mathbf{S}^1 \times \mathbb{C}$ is the following:

$$\begin{aligned} \dot{p} &= e^{i\varphi} f(q) \\ \dot{\varphi} &= F^{\varphi}(q) \\ \dot{q} &= F^{q}(q). \end{aligned} \tag{1.0.2}$$

The proof of this is simple and will be stated in the first section.

In the system 1.0.2, the variable p describes the position of a point in the spiral called the *spiral tip*. This point may be any point in the spiral which keeps the same position with respect to the general structure of the spiral wave. The qualitative dynamics of the system (1.0.2) will depend on the choice of the spiral tip. For example, a spiral tip further from the center of rotation will result in a bigger radius of rotation. Thus it might be preferable to choose a point as close to the center of rotation as possible, especially if we want to observe a petal shaped trajectory. In figure 1.1, the curve shown will most likely be a level curve for a certain value of the wave function. In that case we may choose the spiral tip to be the point on this curve with maximal curvature. It is important to point out that there is no official way to define the spiral tip. Indeed it may change from paper to paper, but each must be consistent with its predetermined definition.

Up to this point, all mathematical research mentioned above consider spiral waves under full $\mathbf{SE}(2)$ symmetry and on unbounded domains. But in experiments where such symmetry might be broken, several new phenomenon occured that could not be explained with the model (1.0.2). We needed to implement perturbations in our system:

$$\frac{\partial u}{\partial t}(x, y, t) = D\nabla^2 u(x, y, t) + \mathcal{F}(u(x, y, t), \lambda) + \varepsilon G(u(x, y, t), \lambda, \varepsilon), \tag{1.0.3}$$

which in turn induces symmetry-breaking perturbation terms G^p, G^{φ} and G^q in the equations of $\dot{p}$, $\dot{\varphi}$ and $\dot{q}$ respectively. For example, the equation for $\dot{\varphi}$ would become

$$\dot{\varphi} = F^{\varphi}(q) + \varepsilon G^{\varphi}(p, \varphi, q, \varepsilon),$$

for $u = p, \varphi, q$, ε is a real perturbation parameter. In this perturbed system, F preserves Euclidian symmetry, but not G. An article by LeBlanc and Wulff [15] tackles the effect of perturbations that break the symmetry of translations, but preserves full rotation symmetry. This is useful in order to emulate boundary effects or the role of localized inhomogeneities in the medium, for example arteries in cardiac tissue, to spiral waves. Specifically, boundary drifting, when spirals drift along boundary of the medium, for example the edge of a petri dish, and spiral anchoring, when the spiral follows an inhomogeneity until it rejoins another cyclic orbit above or below the inhomogeneity, were studied in [23] and [23, 16] respectively. The results obtained in [15] were in some agreement to this. Under the perturbation, only specific periodic solutions exist and they either attract or repel intermediate solutions. Figure 1.3 describes approximate trajectories of a boundary drifting wave in a) and an anchored wave in b), with the inhomogeneity represented in pink.

Subsequent work done by LeBlanc [13] and LeBlanc and Roth [14] investigated the effect of rotation symmetry breaking perturbations and what they found was a phenomenon called phase-locking (see also Lamb and Wulff [12] for another study in an anisotropic medium). Meandering solutions undergoing phase locking have a rational ratio of both the general circular motion frequency and the meandering motion frequency. This has the effect of yielding periodic solutions where generically only quasi-periodic solutions existed in the unperturbed case. Moreover, for each ratio of frequencies, a region was described where phase locking takes place. These regions are called Arnol'd tongues and approach a single point when ε goes to 0. These findings were confirmed in several simulations of the perturbed reaction diffusion system [14, 17, 18].

The next step, which would bring us closer to real world inhomogeneities modeling, would be to study perturbations that break both translational and rotational symmetry and this is the focus of this work. Some previous research has been made in this direction. For example, in [5] the effect of multiple simultaneous localized

perturbations was analyzed. Each of the perturbations broke translation symmetry, but were locally symmetric under rotation around some point. The inclusion of these perturbations had the effect to break rotation and translation symmetry. In this case, spiral anchoring was also observed, as well as hysteresis, where the system suddenly changes its state as a parameter is changed, but does not return to the original state as the parameter change is reversed.

The work presented in this thesis investigates the effect of another perturbation which combines the effects of rotation and translation-breaking symmetry: the lattice perturbation. This specific type of perturbation is only invariant under translations of integer multiples of a certain measure in either of two orthogonal directions, which we will assume to be parallel to the x and y-axes in the $\mathbb{R}^2$ plane, and under rotations of angle $\frac{\pi}{2}$. This represents the symmetries of a standard square grid and for the simplicity of future formulas we will assume that the length of each square is 2π. The motivation to use this perturbation is that the cell structure in various two-dimensional biological tissue is often approximately distributed in a lattice pattern and therefore not homogeneous under $\mathbf{SE}(2)$. Gap junctions [11] and the visual cortex [6] are a good example of such arrangements.

What we present here, however, is but a humble introduction to the problem, as we will only study rigidly rotating or linearly travelling waves, solutions of the simplified system

$$\begin{aligned}\dot{p} &= e^{i\varphi}[v + \varepsilon G^p(p, \varphi, \varepsilon)] \\ \dot{\varphi} &= \omega + \varepsilon G^\varphi(p, \varphi, \varepsilon),\end{aligned}$$

where G^p and G^φ will assume specific forms compatible with lattice symmetry, to be determined later.

The thesis is organized as follows. The next section will go through the formulation of the general $\mathbf{SE}(2)$-invariant system as well as the action of the symmetry group on the function space which constitues the system. After that, the general

form of the Fourier series of the perturbation terms on the center manifold will be established using the symmetries of the lattice. Sections 4 and 5 will analyze perturbed rigidly rotating spiral waves: the former with analytical tools and the latter with numerical simulations to demonstrate the findings. Sections 6 and 7 will analyze perturbed linearly travelling waves in the same fashion. The document will end with a section with concluding remarks.

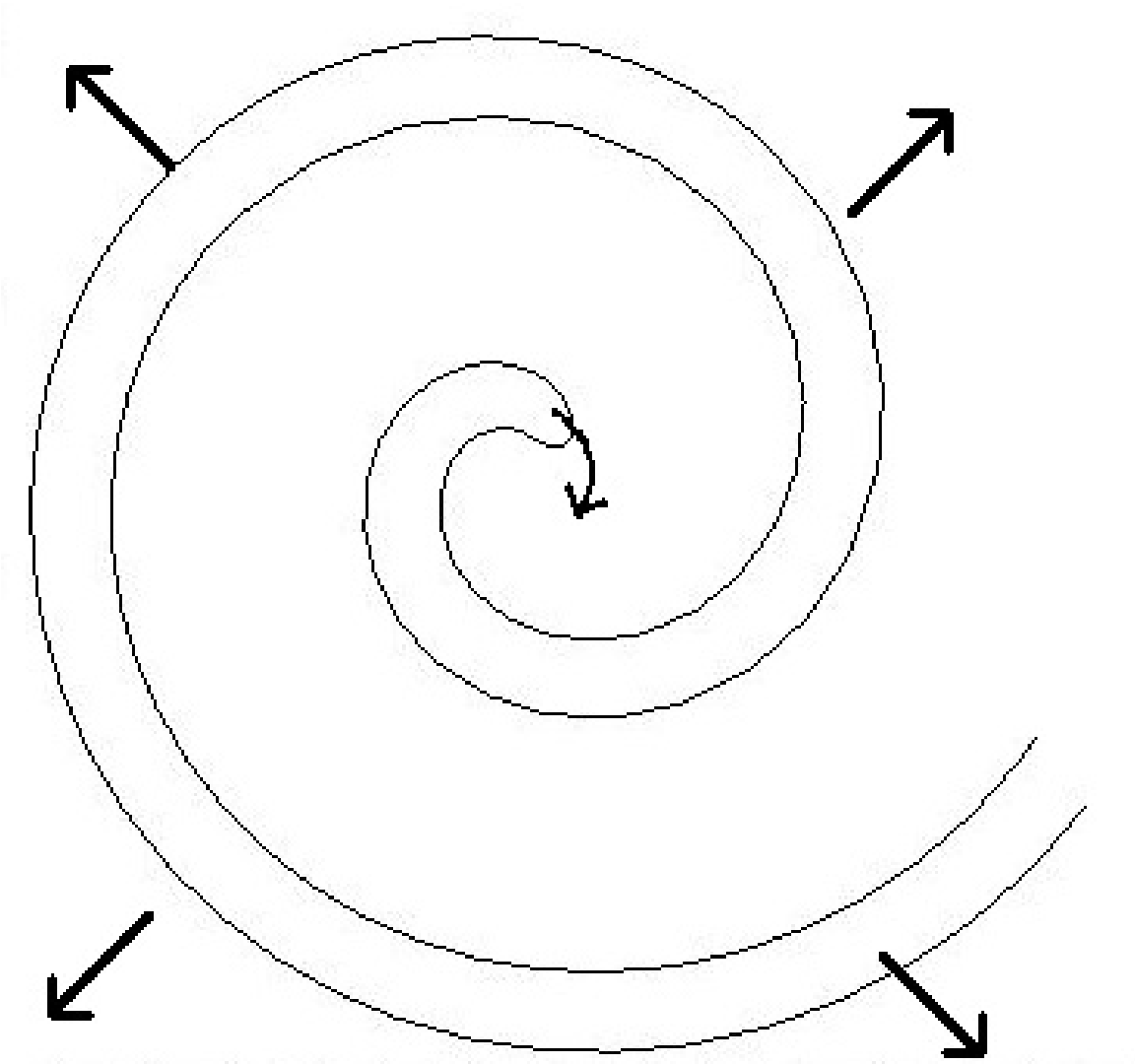

Figure 1.1: Schematic representation of a spiral wave wavefront.

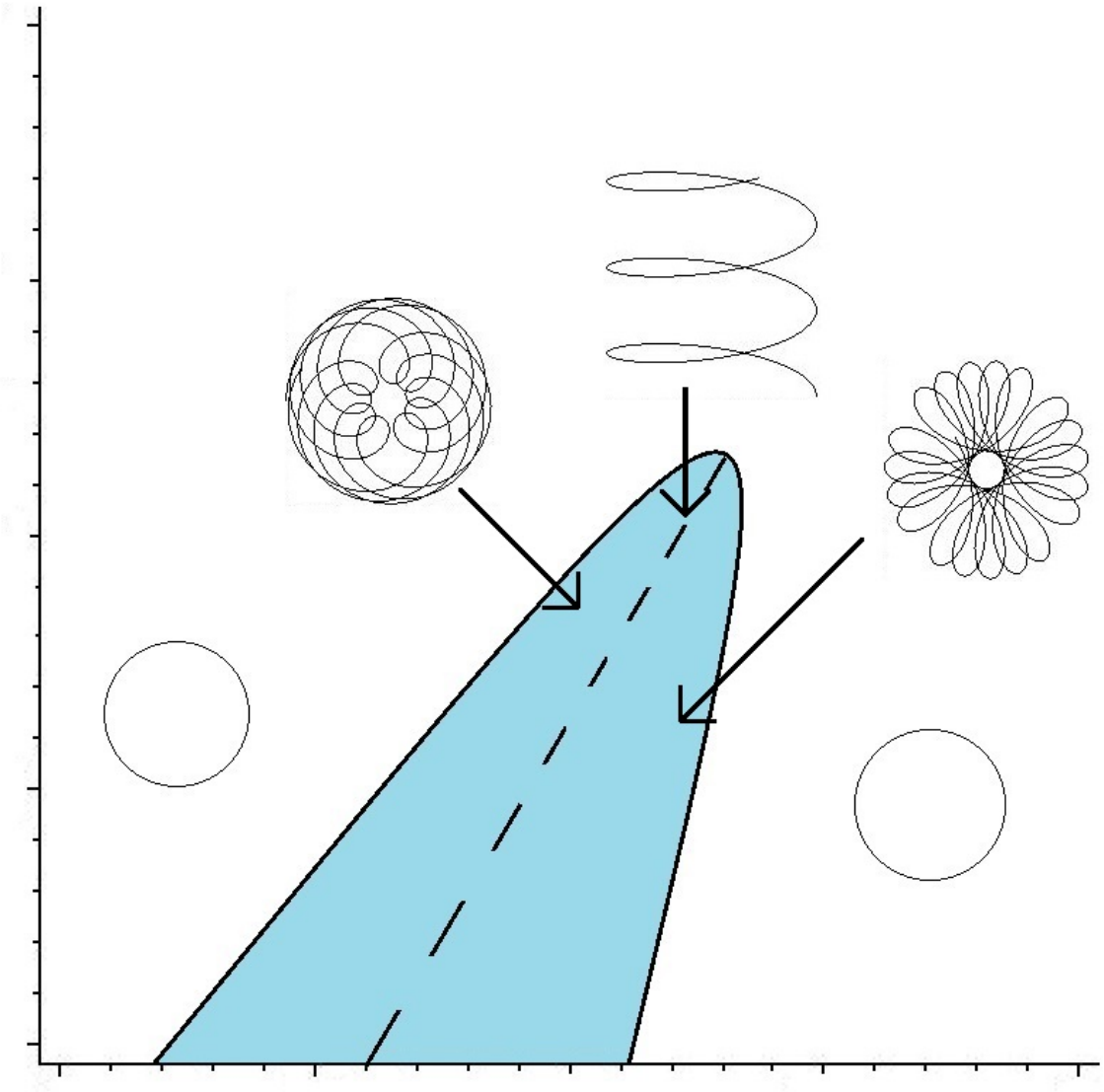

Figure 1.2: Schematic representation of the bifurcation diagram of a spiral wave solution for equation (1.0.1) along with associated approximate trajectories.

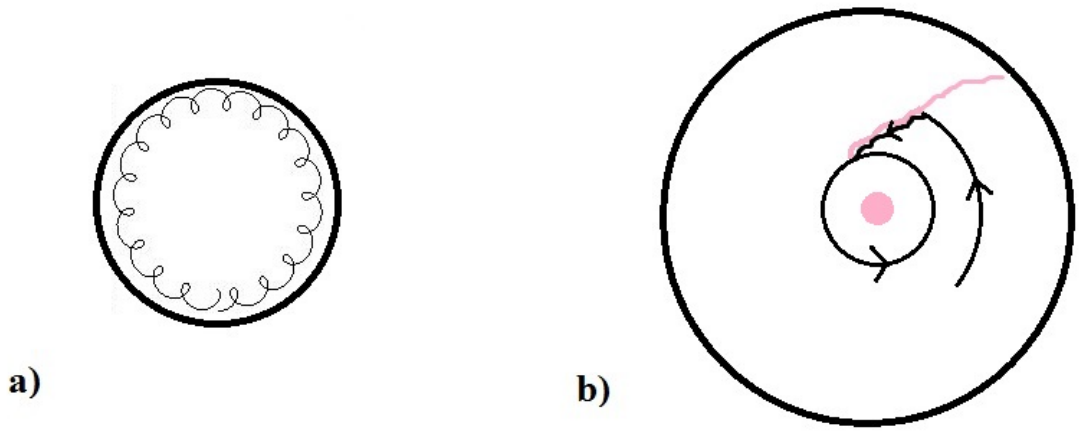

Figure 1.3: Schematic representations of the motion of the spiral tip of a boundary drifting wave (a) and a spiral anchored wave (b).

Chapter 2

Preliminaries: Invariant Equations and Group Action

In this first section, we go through the steps to derive invariant equations under the action of the group **SE**(2). This is a standart result from [20, 21, 8] and will be useful in order to understand the basic dynamics of the spiral tip and to find the most general formulation of our perturbation terms. We will also introduce the definition of the group action of the group **SE**(2).

We already mentioned in the introduction that the equation (1.0.1) must possess **SE**(2) symmetry. Specifically, we have the following property:

$$\begin{gathered}\text{If } u(x,y,t) \text{ is a solution to (1.0.1), then so is} \\ v(x,y,t) = u(x\cos\theta - y\sin\theta + p_1, x\sin\theta + y\cos\theta + p_2, t), \qquad (2.0.1) \\ \text{for any } \theta \in \mathbf{S}^1 \text{ and any } (p_1,p_2) \in \mathbb{R}^2.\end{gathered}$$

In the function space of solutions to (1.0.1), a relative equilibrium is a solution $u(x,y,t)$ such that

$$u(x,y,t) = U_0(x\cos\omega t - y\sin\omega t, x\sin\omega t + y\cos\omega t)$$

for some time-independent function $U_0(x, y)$, or

$$u(x, y, t) = V_0(at, bt)$$

for some time-independent function $V_0(x, y)$. The solutions belonging to the first category are rigidly rotating waves and those belonging to the second are travelling waves.

Because of the symmetry property (2.0.1), these solutions are not isolated in the function space, but are part of a smooth three-dimensional invariant central manifold which is isomorphic to $\mathbb{C} \times \mathbf{S}^1$ [20, 21, 8]. Because the Euclidian symmetry, linearization of (1.0.1) about a relative equilibrium solution yields eigenvalues at 0 and $\pm\omega i$. In this thesis we will assume that all the other eigenvalues and spectrum of this linearization are uniformly bounded away from the imaginary axis in the left-hand plane. It then follows from the center manifold reduction of [8, 20, 21] that the asymptotical dynamics of (1.0.1) near a relative equilibrium are given by an $\mathbf{SE}(2)$-invariant system of ordinary differential equations on the center manifold $\mathbb{C} \times \mathbf{S}^1$. This will be the central object of our analysis in this thesis.

We parametrize the center manifold $\mathbb{C} \times \mathbf{S}^1 \equiv Y$ using a complex variable p and an angular variable φ. It is useful to represent these variables as the position of the spiral tip in physical space and the rotation angle of the spiral wavefront with respect to its axis of rotation. The most general system of ordinary differential equations on Y then becomes:

$$\begin{aligned} \dot{p} &= F^p(p, \varphi) \\ \dot{\varphi} &= F^\varphi(p, \varphi). \end{aligned} \tag{2.0.2}$$

However, in order to comply with the $\mathbf{SE}(2)$-symmetry requirements of (1.0.1), the functions F^p and F^φ will not be completely arbitrary. Let $(x, \theta) \in \mathbf{SE}(2) \cong \mathbb{C} \times \mathbf{S}^1$ and $(p, \varphi) \in Y$. We define the action of the group $\mathbf{SE}(2)$ of translations and rotations

on Y by:

$$(x,\theta)(p,\varphi) = (pe^{i\theta} + x, \varphi + \theta). \tag{2.0.3}$$

Thus, if $(p(t),\varphi(t))$ is a solution of (2.0.2), then so is $(x,\theta)(p(t),\varphi(t))$ for all $(x,\theta) \in$ **SE**(2). This property is analoguous to (2.0.1).

If the equations (2.0.2) must be invariant for all the possible transformations (2.0.3), they must be for only one of these. Let's begin with a simple translation:

$$(p,\varphi) \mapsto (p + x, \varphi) \tag{2.0.4}$$

In order for (2.0.2) to be invariant under translations (2.0.4), these functions must be invariant in the true sense of the term. i.e.

$$F^p(p + x, \varphi) = F^p(p,\varphi)$$
$$F^\varphi(p + x, \varphi) = F^\varphi(p,\varphi),\ \forall x \in \mathbb{C}.$$

This means that F^p and F^φ must be functions of φ only.

For rotation, the symmetry imposes the following conditions:

$$F^p(\varphi + \theta) = e^{i\theta}F^p(\varphi) \tag{2.0.5}$$
$$F^\varphi(\varphi + \theta) = F^\varphi(\varphi).$$

This can be explained by visualizing the velocity vectors of our system. Let the system be in the cartesian plane, then the velocity vector is in this same plane. This vector is invariant for translations, as moving both its extremities in the same direction leaves it unchanged, but a rotation will change its direction, hence the $e^{i\theta}$ factor. For the angular velocity vector, its vector is represented as orthogonal to the cartesian plane, so neither transformation will affect it. Returning to the functions F^p and F^φ, we observe that the latter does not depend on φ, so it is a constant ω. In the case of F^p, define $H(\varphi) = e^{-i\varphi}F^p(\varphi)$, and we obtain

$$H(\varphi+\theta) = e^{-i\varphi}e^{-i\theta}e^{i\theta}F^p(\varphi) = e^{-i\varphi}F^p(\varphi) = H(\varphi).$$

We can now conclude that H is independent of φ. The system (2.0.2) becomes

$$\begin{aligned} \dot{p} &= ve^{i\varphi} \\ \dot{\varphi} &= \omega, \end{aligned} \tag{2.0.6}$$

where v is a complex constant, ω is a real constant. This system of ordinary differential equations corresponds to the most general form of spiral wave dynamics at a relative equilibrium, in a purely Euclidian context. We can easily recognize the rotating wave system as the case when $\omega \neq 0$ and the travelling wave as the case when $\omega = 0$. In practice, the Euclidian case is not always ideal when dealing with impurities or limited environment. This is the reason why we add perturbation terms to our systems, as will be done in the next chapter. However, before we get knee-deep into Fourier series expansions and further analysis, we shall introduce the different notations used in this thesis.

2.1 Notation

Since we are working with the variable $p \in \mathbb{C}$, which corresponds to the position of the spiral tip on a two-dimensional plane, we choose three different notations to represent its value. The first one is to keep the complex form of $p = x+iy$. This notation is the most compact and rotations by an angle θ are easily written as $e^{i\theta}p$. Its drawbacks are that its derivatives can become ambiguous, as we shall need the derivative in $\mathbb{R}^2$, the jacobian matrix, instead of the complex derivative. This is why we introduce the matrix notation. In this notation, p becomes $X = \begin{pmatrix} x \\ y \end{pmatrix} \in \mathbb{R}^2$, rotations become a matrix operator $R_\varphi = \begin{pmatrix} \cos\varphi & -\sin\varphi \\ \sin\varphi & \cos\varphi \end{pmatrix}$. Using this notation we can clearly find the

derivative of a function $F = \begin{pmatrix} f_1(x,y) \\ f_2(x,y) \end{pmatrix}$ with the jacobian matrix $Df = \begin{pmatrix} \frac{\partial f_1}{\partial x} & \frac{\partial f_1}{\partial y} \\ \frac{\partial f_2}{\partial x} & \frac{\partial f_2}{\partial y} \end{pmatrix}$. The third and final notation is the coordinates notation, in which we separate the real and imaginary parts of p into two real variables x and y. This notation is the least compact and can get bothersome very quickly to the point that we need to get equations of a reasonable size. The advantage of the coordinates notation is that it is the easiest to use in numerical simulations. As many of the results in this thesis will be reproduced in numerical experiments, we shall write results using this last notation if possible. Table 2.1 gives a general overview of the notations.

Notation	Position of the spiral tip	Rotation by angle θ	Functions
Complex	$p = x + iy$	$e^{i\theta}p$	$f(x+iy) = f_1(x,y) + if_2(x,y)$
Matrix	$X = \begin{pmatrix} x \\ y \end{pmatrix}$	$R_\varphi X = \begin{pmatrix} \cos\varphi & -\sin\varphi \\ \sin\varphi & \cos\varphi \end{pmatrix} \begin{pmatrix} x \\ y \end{pmatrix}$	$F(X) = \begin{pmatrix} f_1(x,y) \\ f_2(x,y) \end{pmatrix}$
Coordinates	$x = \mathrm{Re}\ p$ $y = \mathrm{Im}\ p$	$x = \cos\theta\ \mathrm{Re}\ p - \sin\theta\ \mathrm{Im}\ p$ $y = \cos\theta\ \mathrm{Im}\ p + \sin\theta\ \mathrm{Re}\ p$	$f_1(x,y)$ $f_2(x,y)$

Table 2.1: Table showing the three notations with respect to the position of the spiral tip, rotations and functions.

Chapter 3

Perturbations Associated to a Discretization of Space

Discretization of space in a lattice pattern is one of the factors which could influence the behavior of a spiral wave. As mentioned in the introduction, the lattice perturbation could represent the regular array of gap junctions between cells in a two-dimnesional excitable tissue, like a muscle or a retina. One could also envisage a light-sensitive Belousov-Zhabotinsky reaction exposed to an array of lasers. Finally one could argue that studying spiral waves under lattice perturbation could serve as a middle ground between the fully Euclidian partial differential equation (1.0.1) and the lattice dynamical system generated by the discretization of space in a numerical simulation of that same system. This last point is still tenuous and would require further investigation beyond the scope of this thesis.

To observe the effects of the perturbation, we must define our symmetries and then adapt equation (2.0.6) to them. Regarding the symmetries, the remaining translation symmetries are those by an integer multiple of one unit in two predetermined orthogonal directions. We shall fix this unit to 2π and the directions to the real and imaginary axes respectively. Rotation symmetry is then only limited to angles of $\frac{\pi}{2}$.

These are the symmetries of an orthogonal grid. To reflect this modification to our system, we add a perturbation term [7, 13, 15] to each of our equations in (2.0.6):

$$\begin{aligned} \dot{p} &= e^{i\varphi}(v + \varepsilon G^p(x, y, \varphi, \varepsilon)) \\ \dot{\varphi} &= \omega + \varepsilon G^{\varphi}(x, y, \varphi, \varepsilon), \end{aligned} \tag{3.0.1}$$

where x and y are the real and imaginary part of p respectively and ε is a small, real and positive perturbation parameter. Note that we already factorized $e^{i\varphi}$ out of G^p. This means that G^p will need to be completely invariant on $x, y \in 2\pi\mathbb{Z}$ and $\varphi \in \frac{\pi}{2}\mathbb{Z}$, that is $G^p(x, y, \varphi, \varepsilon) = G^p(x\cos\frac{n\pi}{2} - y\sin\frac{n\pi}{2} + l2\pi, y\cos\frac{n\pi}{2} + x\sin\frac{n\pi}{2} + m2\pi, \varphi + \frac{n\pi}{2}, \varepsilon)$, for $l, m \in \mathbb{Z}$, $n = 0, 1, 2, 3$. It then follows that G^p and G^{φ} must be 2π-periodic in x, y and φ. For this reason we may assume the phase space for solutions of (3.0.1) is in fact a three-torus T^3. We may write the functions G^p and G^{φ} (denoted in general as G here) as a Fourier series

$$G(x, y, \varphi, \varepsilon) = \sum_{j,k,l\in\mathbb{Z}} A_{jkl}(\varepsilon) e^{i(j\varphi + kx + ly)} \tag{3.0.2}$$

and after applying a $\frac{\pi}{2}$ space-time rotation, which preserves the spiral, G becomes

$$G(-y, x, \varphi + \frac{\pi}{2}, \varepsilon) = \sum_{j,k,l\in\mathbb{Z}} A_{jkl}(\varepsilon) e^{i(j\varphi - ky + lx + j\frac{\pi}{2})}.$$

By symmetry, these two equations must be equal, generating the following condition:

$$A_{j,k,l}(\varepsilon) = A_{j,-l,k}(\varepsilon) e^{ij\frac{\pi}{2}}.$$

This leads to four categories of perturbation terms, each harboring two families of solutions. The first, when $j = 4m$, $m \in \mathbb{Z}$ gives

$$A_{j,k,l}(\varepsilon) = A_{j,-l,k}(\varepsilon) = A_{j,-k,-l}(\varepsilon) = A_{j,l,-k}(\varepsilon).$$

A term in (3.0.2) associated to A_{ijk} has the following form:

$$A_{ijk}(\varepsilon) e^{i4m\varphi}(e^{i(kx+ly)} + e^{-i(kx+ly)} + e^{i(lx-ky)} + e^{-i(lx-ky)})$$

$$= A_{ijk}(\varepsilon)e^{i4m\varphi}(2\cos(kx+ly)+2\cos(lx-ky)).$$

Taking real and imaginary parts of this result, we get the first two families of solutions:

i. $\cos(4m\varphi)(\cos(kx+ly)+\cos(lx-ky))$

ii. $\sin(4m\varphi)(\cos(kx+ly)+\cos(lx-ky))$.

Note that while we only list real solutions, any linear combination of solutions with complex coefficients is also a solution. In a similar fashion, we find the solution to the other families. The second category is when $j = 4m+1$ and we obtain the constraint:

$$A_{j,k,l}(\varepsilon) = iA_{j,-l,k}(\varepsilon) = -A_{j,-k,-l}(\varepsilon) = -iA_{j,l,-k}(\varepsilon).$$

The associated term in (3.0.2) becomes

$$\begin{aligned} &A_{ijk}(\varepsilon)e^{i(4m+1)\varphi}(e^{i(kx+ly)} - e^{-i(kx+ly)} - ie^{i(-lx+ky)} + ie^{-i(-lx+ky)}) \\ &\quad = A_{ijk}(\varepsilon)e^{i(4m+1)\varphi}(2i\sin(kx+ly) - 2\sin(lx-ky)) \end{aligned}$$

and we obtain the real solutions:

iii. $\sin((4m+1)\varphi)\sin(kx+ly)+\cos((4m+1)\varphi)\sin(lx-ky)$

iv. $\cos((4m+1)\varphi)\sin(kx+ly)-\sin((4m+1)\varphi)\sin(lx-ky)$.

The third category corresponds to $j = 4m+2$:

$$A_{j,k,l}(\varepsilon) = -A_{j,-l,k}(\varepsilon) = A_{j,-k,-l}(\varepsilon) = -A_{j,l,-k}(\varepsilon),$$

which yields

$$\begin{aligned} &A_{ijk}(\varepsilon)e^{i(4m+2)\varphi}(e^{i(kx+ly)} + e^{-i(kx+ly)} - e^{i(-lx+ky)} - e^{-i(-lx+ky)}) \\ &\quad = A_{ijk}(\varepsilon)e^{i(4m+2)\varphi}(2\cos(kx+ly) - 2\cos(lx-ky)) \end{aligned}$$

and

v. $\cos((4m+2)\varphi)(\cos(kx+ly)-\cos(lx-ky))$

vi. $\sin((4m+2)\varphi)(\cos(kx+ly)-\cos(lx-ky))$.

Finally, the fourth category corresponds to $j = 4m+3$ and we get

$$A_{j,k,l}(\varepsilon) = -iA_{j,-l,k}(\varepsilon) = -A_{j,-k,-l}(\varepsilon) = iA_{j,l,-k}(\varepsilon),$$

$$\begin{aligned} &A_{ijk}(\varepsilon)e^{i(4m+3)\varphi}(e^{i(kx+ly)} - e^{-i(kx+ly)} + ie^{i(-lx+ky)} - ie^{-i(-lx+ky)}) \\ &\quad = A_{ijk}(\varepsilon)e^{i(4m+3)\varphi}(2i\sin(kx+ly) + 2\sin(lx-ky)) \end{aligned}$$

and

vii. $-\sin((4m+1)\varphi)\sin(kx+ly) + \cos((4m+1)\varphi)\sin(lx-ky)$

viii. $\cos((4m+1)\varphi)\sin(kx+ly) + \sin((4m+1)\varphi)\sin(lx-ky)$.

We now have the general algebraic forms for the perturbation terms in (3.0.1), grouped in eight distinct families. This allows us to observe the behavior of the spiral tip under these perturbations in numerical analysis.

Chapter 4

Perturbed Rotating Waves

In this section we will perform a theoretical analysis of the system of equations (3.0.1) in the case when $\omega \neq 0$ and $0 < \varepsilon \ll \omega$. The solutions to this system will be interpreted as the motion of the spiral tip in a reaction-diffusion system (1.0.1) in a symmetry-breaking environment which only preserves lattice symmetries.

4.1 Behavior of the Perturbed System: Anchored Rotating Waves

In the purely Euclidian case when $\varepsilon = 0$ and $\omega \neq 0$, all solutions are periodic. This suggests that for a non-zero ε, but small relative to ω, we seek periodic solutions of (3.0.1). In this situation, φ is always increasing (assuming without loss of generality that $\omega > 0$), so we can then recalibrate time in (3.0.1) to obtain the following orbitally equivalent system:

$$\begin{aligned} \dot{p} &= e^{i\varphi}(v + \varepsilon G_1^p(x, y, \varphi, \varepsilon)) \\ \dot{\varphi} &= 1. \end{aligned} \tag{4.1.1}$$

This allows us to concentrate on a single variable p and to use φ as a measure of time. We shall search for periodic solutions of (4.1.1). On these solution curves if we take a point $p(t_0)$ and look at it 2π later, we find it at the exact same location:

$$p(t_0 + 2\pi) = p(t_0).$$

While this is true for all points in the Euclidian case, it is not necessarily true in the perturbed case. We must then formulate a Poincaré map, giving the position of a point after each revolution in φ. We formally define the map as the next point of intersection of the solution with the surface $\varphi = 0$ from a point on that same surface. We then say that the map has a *Poincaré section* $\varphi = 0$. To achieve this we intergrate the Taylor series of $\dot{p}$ near $\varepsilon = 0$.

$$\begin{aligned} p(\varphi, \varepsilon) &= p(0) + \int_0^{\varphi} \dot{p}(s, \varepsilon) ds = p(0) + \int_0^{\varphi} e^{is}(v + \varepsilon G_1^p(x, y, s, \varepsilon)) ds \\ &= p_0(\varphi) + \varepsilon p_1(\varphi) + O(\varepsilon^2) \end{aligned}$$

where $O(\varepsilon^2)$ indicates terms of order two or higher. The first term of the series is

$$\begin{aligned} p_0(\varphi) =& p(0) + \int_0^{\varphi} v e^{is} ds = p(0) + iv(1 - e^{i\varphi}) \\ =& x(0) + \mathrm{Im}(v)(\sin(\varphi) - 1) + \mathrm{Re}(v)\cos(\varphi) \\ &+ i(y(0) + \mathrm{Re}(v)(1 - \cos(\varphi)) + \mathrm{Im}(v)\sin(\varphi)) \\ =& x(\varphi, 0) + iy(\varphi, 0) \end{aligned}$$

and we have $p(2\pi, 0) = p(0, 0)$ as specified. The second term of the series is obtained by differentiating with respect to ε at $\varepsilon = 0$ and we obtain

$$p_1(\varphi) = \int_0^{\varphi} e^{is} G_1^p(x(s, 0), y(s, 0), s, 0) ds \tag{4.1.2}$$

We now have our Poincaré map if we integrate up to 2π and it has the form $p + \varepsilon H(x, y, \varepsilon)$ with the first Taylor coefficient of H centered at $\varepsilon = 0$ being $H(x, y, 0) =$

$p_1(2\pi)$. The complex function $H(x, y, 0)$ can then be separated into its real part and imaginary part $H(x, y, 0) = f_1 + if_2$ as follows:

$$\begin{aligned} f_1(x,y) = &\int_0^{2\pi} \cos(s)\mathrm{Re}(G_1^p(x(s,0), y(s,0), s, 0)) \\ &- \sin(s)\mathrm{Im}(G_1^p(x(s,0), y(s,0), s))ds \\ f_2(x,y) = &\int_0^{2\pi} \cos(s)\mathrm{Im}(G_1^p(x(s,0), y(s,0), s, 0)) \\ &+ \sin(s)\mathrm{Re}(G_1^p(x(s,0), y(s,0), s))ds. \end{aligned}$$

This way, we can consider H as a function of $\mathbb{R}^3$ into $\mathbb{R}^2$ and to first order, fixed points of the Poincaré map correspond to coordinates x_{eq}, y_{eq} where $H(x_{eq}, y_{eq}, 0) = 0$. Without any more information on the perturbation, we cannot compute directly those equilibrium points; however we can find clues about their existence. Indeed by the symmetries of the system of ordinary differential equations, zeroes of $H(x, y, 0))$ come in families of four. To see this, we need a change of coordinates. Let $q = Q(p) = p+iv$; we therefore get $Q^{-1}(q) = q - iv$ and we can compute $H(x, y, 0)$ (using the complex notation $H(p, 0)$) in these new coordinates:

$$\begin{aligned} Q(Q^{-1}(q) + \varepsilon H(Q^{-1}(q), 0)) &= iv + q - iv + \varepsilon H(q - iv, 0) \\ &= q + \varepsilon \int_0^{2\pi} e^{is} G_1^p(q - iv + iv - ive^{is}, s, 0)ds \\ &= q + \varepsilon \int_0^{2\pi} e^{is} G_1^p(q - ive^{is}, s, 0)ds = P(q, \varepsilon), \end{aligned}$$

where P is our first-order Poincaré map in the new coordinates. If we have a fixed point p_0 of the first-order Poincaré map in the old coordinates, then $P(Q(p_0), \varepsilon) = Q(p_0)$. Now an examination of $P(iq, \varepsilon), q \in \mathbb{C}$ gives us

$$P(iq, \varepsilon) = iq + \varepsilon \int_0^{2\pi} e^{is} G_1^p(i(q - ve^{is}), s, 0)ds = iq + \varepsilon \int_0^{2\pi} e^{is} G_1^p(e^{i\frac{\pi}{2}}(q - ve^{is}), s, 0)ds$$

by applying the symmetry of G_1^p for $\frac{\pi}{2}$ angles, and applying the substitution $s \mapsto s - \frac{\pi}{2}$,

$$P(iq, \varepsilon) = iq + \varepsilon \int_0^{2\pi} e^{is} G_1^p(e^{i\frac{\pi}{2}}(q - ve^{is}), s, 0)ds$$

$$= iq + \varepsilon \int_0^{2\pi} e^{is} G_1^p(q - ve^{is}, s - \frac{\pi}{2}, 0)ds$$
$$= iq + i\varepsilon \int_{\frac{-\pi}{2}}^{\frac{3\pi}{2}} e^{is} G_1^p(q - ive^{is}, s, 0)ds = iP(q, \varepsilon).$$

The same argument can also be used for higher order terms in the full Poincaré map. Thus if $Q(x_0, y_0)$ is a fixed point of P, then so is $e^{i\frac{\pi}{2}}Q(x_0, y_0)$. By repeating this process, we obtain in general a family of four solutions. It can be represented by $e^{i\frac{n\pi}{2}}Q(x_0, y_0)$, $n = 0, 1, 2, 3$. These solutions are distinct when $Q(x_0, y_0)$ is different from the origin or the point (π, π).

Theorem 4.1.1. *Let x_0, y_0 be in $\mathbb{R}$ such that $H(x_0, y_0, 0) = 0$ and*

$$D_{(x,y)}H(x_0, y_0, 0) = \left(\frac{\partial f_1}{\partial x}\frac{\partial f_2}{\partial y} - \frac{\partial f_1}{\partial y}\frac{\partial f_2}{\partial x}\right)(x_0, y_0, 0) \neq 0,$$

then there exists, for small ε, a solution $H(x(\varepsilon), y(\varepsilon), \varepsilon) = 0$. Moreover, each fixed point is associated to a family of four other fixed points, obtained via $\frac{\pi}{2}$ rotations, i.e.

$$P(e^{i\frac{n\pi}{2}}Q(x(\varepsilon), y(\varepsilon))) = e^{i\frac{n\pi}{2}}Q(x(\varepsilon), y(\varepsilon)), \quad n = 0, 1, 2, 3.$$

One such family of interest is found when $Q(x_0, y_0) = 0$. In that case the property yields

$$P(0) = P(iQ(x_0, y_0)) = iP(Q(x_0, y_0)),$$

therefore $P(Q(x_0, y_0)) = 0$. This solution is important as its projection in the xy-plane will exhibit a spatio-temporal symmetry by rotations of $\frac{\pi}{2}$. We will show an example of such a solution later.

We also need to point out that the transformation Q will depend on the choice of surface used for the Poincaré map. Its role is to study the evolution of the center of rotation of the solution instead of some point that crosses the surface. In our case, when the solution meets the surface, we know that its φ value is zero and that its position with relation to the center of rotation will stay the same. If we had chosen

any other $\varphi = \varphi_p$ type surface as our Poincaré section, we would have needed to use $Q(p) = p + ie^{i\varphi_p}v$.

Proof: (**Proof of theorem 4.1.1**)

The implicit function theorem states that if the Jacobian matrix of H restricted to $\varepsilon = 0$ is invertible, which is the case here, then there exists, for ε small enough, differentiable functions $x(\varepsilon)$ $y(\varepsilon)$ such that $H(x(\varepsilon), y(\varepsilon)) = 0$. The second part of the theorem arises from the symmetries of the system and was demonstrated earlier. ∎

This principle can be better understood by observing the level sets corresponding to $f_1(x, y, 0) = 0$ et $f_2(x, y, 0) = 0$. The fixed points are their intersection points. If $\frac{\partial f_1}{\partial x}\frac{\partial f_2}{\partial y} - \frac{\partial f_1}{\partial y}\frac{\partial f_2}{\partial x} \neq 0$ at a fixed point, the curves cross transversely and a small change in ε will not make the fixed point dissapear; it will only move it slightly. However, if $\frac{\partial f_1}{\partial x}\frac{\partial f_2}{\partial y} - \frac{\partial f_1}{\partial y}\frac{\partial f_2}{\partial x} = 0$, the curves are tangent at the fixed point and it may vanish if we introduce a perturbation, as small as it may be. The previous theorem gives us a formula to easily verify the existence of periodic solutions in the perturbed system.

4.2 Stability of the Relative Equilibria

Now that we obtained some conditions for the existence of periodic solutions in (4.1.1), the next step would be to determine their stability. Since the Poincaré map transforms our problem into a discrete dynamical system with two real variables x and y, we need to find the eigenvalues of the Jacobian matrix of our map, defined by:

$$p(x, y, \varepsilon) = p + \varepsilon H(x, y, 0) + O(\varepsilon^2).$$

If these eigenvalues have a modulus less than 1, the orbit is asymptotically stable. If the modulus of either one of the eigenvalues is greater than 1, it is unstable. The

Jacobian matrix of p is

$$J_p = \begin{pmatrix} 1+\varepsilon\frac{\partial f_1}{\partial x} & \varepsilon\frac{\partial f_1}{\partial y} \\ \varepsilon\frac{\partial f_2}{\partial x} & 1+\varepsilon\frac{\partial f_2}{\partial y} \end{pmatrix} + O(\varepsilon^2),$$

the eigenvalues are the solution of the characteristic polynomial

$$\lambda^2 - \mathrm{Tr}(J_p)\lambda + \det(J_p) = 0$$

$$\lambda = \frac{\mathrm{Tr}(J_p)}{2} \pm \frac{\sqrt{\mathrm{Tr}(J_p)^2 - 4\det(J_p)}}{2}.$$

However if we compute λ in the case when $\varepsilon = 0$, we obtain $\lambda = 1$ as the only eigenvalue and no conclusion can be established for the stability of periodic orbits. This was to be expected, as all points in the Euclidian system already lie on a periodic orbit. As a result, the effect of the perturbation in the $0 < \varepsilon \ll \omega$ on λ will dictate the stability of periodic orbits.

Now, rather than trying to figure out the conditions for $|\lambda|$ to be superior or inferior to 1, we will look at the value of the eigenvalues μ of J_H, the Jacobian matrix of H:

$$J_H = \begin{pmatrix} \varepsilon\frac{\partial f_1}{\partial x} & \varepsilon\frac{\partial f_1}{\partial y} \\ \varepsilon\frac{\partial f_2}{\partial x} & \varepsilon\frac{\partial f_2}{\partial y} \end{pmatrix} + O(\varepsilon^2).$$

Indeed, if λ is an eigenvalue of J_p, then $\mu = \lambda - 1$ is an eigenvalue of J_H because $J_p = J_H + I_2$, where I_2 is the two by two identity matrix. The value of μ is the variation of the eigenvalues from the perturbed system to the Euclidian system. If its real part is locally negative , $|\lambda|$ becomes less than one and we have a stable periodic orbit. Inversely a positive real part for μ results in an unstable solution. We also know that the trace of a square matrix is equal to the sum of its eigenvalues and its determinant is equal to the product of the eigenvalues. If both values of μ have negative real part, then $\tau = \mathrm{Tr}(J_H)$ must be inferior to zero and $\delta = \mathrm{Det}(J_H)$ must be positive. On the other hand if either $\tau > 0$ or $\delta < 0$, then both eigenvalues μ have positive real part. Since μ is of order of at least ε, we will assume that the real part

of μ will be in a close neighbourhood of 0, close enough that if μ has negative real part, then $|\lambda| < 1$.

Computing the values of $\tau =$ and δ yields

$$\tau = \mathrm{Tr}(J_H) = \varepsilon \left(\frac{\partial f_1}{\partial x} + \frac{\partial f_2}{\partial y} \right) + O(\varepsilon^2)$$
$$\delta = \mathrm{Det}(J_H) = \varepsilon^2 \left(\frac{\partial f_1}{\partial x}\frac{\partial f_2}{\partial y} - \frac{\partial f_1}{\partial y}\frac{\partial f_2}{\partial x} \right) + O(\varepsilon^3).$$

For ε small enough, the term of highest order dominates the others and thus determines the sign of τ and δ. For the former value, it is the ε term and in the latter it is the ε^2 one. Let τ and δ be these dominant terms respectively. We then have the following theorem.

Theorem 4.2.1. *Let x_0, y_0 be the coordinates of a fixed point of the Poincaré map $p(x, y, \varepsilon) = x+iy+\varepsilon(f_1(x, y, \varepsilon)+if_2(x, y, \varepsilon))$, then if $\tau = \frac{\partial f_1}{\partial x}+\frac{\partial f_2}{\partial y} < 0$ and $\delta = \frac{\partial f_1}{\partial x}\frac{\partial f_2}{\partial y} - \frac{\partial f_1}{\partial y}\frac{\partial f_2}{\partial x} > 0$, then the periodic solution of (4.1.1) containing (x_0, y_0) is asymptotically stable. If either $\tau > 0$ or $\delta < 0$ then the periodic solution is unstable.*

The physical effects of the lattice perturbation on a chemical reaction, for example, will be to anchor or repel the solutions around a specific point in space. That point will either be the center of a lattice-symmetric rotation, in which case the periodic solution will exhibit spatio-temporal symmetry under rotations of $\frac{\pi}{2}$, or around another arbitrary point, in which case rotations of $\frac{\pi}{2}$ of the lattice grid will result in another periodic orbit. Such anchoring along an arbitrary points has also been observed on spiral waves with multiple localized perturbations in [5].

Chapter 5

Examples of $\omega \neq 0$ systems

In the previous chapter, we stated and proved several properties of perturbated rigidly rotating waves. In order to illustrate these properties and also to have a good look at solutions of these systems, we have computed some numerical simulations using the *dsolve* tool with the Fehlberg fourth-fifth order Runge-Kutta method in Maple. To produce these plots, we take a sample of one hundred thousand and one points each separated by the same step size Δt. In order to reproduce the three-torus phase space of (3.0.1) in a plot, we restricted our points to a cube of length 2π and if a solution leaves the cube, we replace it on the opposite side of the cube. For example, if the x value of a point gets to 2π when $y = 3$ and $\varphi = 2$, we move the point to $(x, y, \varphi) = (0, 3, 2)$.

Using the following form of the system (3.0.1):

$$\begin{aligned} \dot{x} &= \cos\varphi(v_x + \varepsilon F_x(x, y, \varphi, \varepsilon)) - \sin\varphi(v_y + \varepsilon F_y(x, y, \varphi, \varepsilon)) \\ \dot{y} &= \sin\varphi(v_x + \varepsilon F_x(x, y, \varphi, \varepsilon)) + \cos\varphi(v_y + \varepsilon F_y(x, y, \varphi, \varepsilon)) \\ \dot{\varphi} &= \omega + \varepsilon G(x, y, \varphi, \varepsilon), \end{aligned} \tag{5.0.1}$$

with Fourier modes as in chapter 3, we show here projections in the xy-plane of the solutions after the transient state has dissipated as well as an example showing that

transient state. The system used to generate figure 5.1 is

$$\begin{aligned}
\dot{x} =& \cos\varphi(1 + 0.2(\sin(5\varphi)\sin(x+y) + \cos(5\varphi)\sin(x-y))) \\
& - \sin\varphi(1 + 0.2\cos(2\varphi)(\cos(2x+3y) - \cos(3x-2y))) \\
\dot{y} =& \sin\varphi(1 + 0.2(\sin(5\varphi)\sin(x+y) + \cos(5\varphi)\sin(x-y))) \\
& + \cos\varphi(1 + 0.2\cos(2\varphi)(\cos(2x+3y) - \cos(3x-2y))) \\
\dot{\varphi} =& 1 + 0.2\sin(12\varphi)(\cos(7x+5y) + \cos(5x-7y)),
\end{aligned} \tag{5.0.2}$$

with initial values $x(0) = 5$, $y(0) = 1$, $\varphi(0) = 0$. With this large value of $\varepsilon = 0.2$, we can readily observe the distortion caused by the perturbation on the solution.

In order to get a better simulation of the effects of a small perturbation, we generated the solution of another system shown in figures 5.2 and 5.3:

$$\begin{aligned}
\dot{x} =& \cos\varphi(1 + 0.05\sin(4\varphi)(\cos(2x+2y) + \cos(2x-2y))) \\
& - \sin\varphi(0.05\sin(4\varphi)(\cos(2x+2y) + \cos(2x-2y))) \\
\dot{y} =& \sin\varphi(1 + 0.05\sin(4\varphi)(\cos(2x+2y) + \cos(2x-2y))) \\
& + \cos\varphi(0.05\sin(4\varphi)(\cos(2x+2y) + \cos(2x-2y))) \\
\dot{\varphi} =& 1 + 0.05(\cos(7\varphi)\sin(x+y) + \sin(7\varphi)\sin(x-y)),
\end{aligned} \tag{5.0.3}$$

with initial values $x(0) = \frac{1}{2}$, $y(0) = 3$, $\varphi(0) = 0$. In figure 5.2, with the smaller value of $\varepsilon = 0.05$, we can no longer distinguish to the naked eye the distorted orbit from the original, Euclidian symmetric one. Note that figure 5.2 was taken after the transient state dissipated. If the transient phase had been added, we could have seen the difference, as the Euclidian solution is always on a periodic orbit and the perturbed solution is generically away from such an orbit initially, but asymptotically approaching it. This is evident if we include the transient phase as in figure 5.3

So far, in all the solutions illustrated, the diameter of the trajectory is always smaller than the 2π square unit of the torus. What if it was much greater? The

system used to generate figure 5.4 is as follows:

$$\begin{aligned}
\dot{x} =& \cos\varphi(5 + 0.1(-\sin(15\varphi)\sin(2x+y) + \cos(15\phi)\sin(1x-2y))) \\
& - \sin\varphi(8 + 0.1(\cos(37\varphi)\sin(6x+7y) - \sin(37\varphi)\sin(7x-6y))) \\
\dot{y} =& \sin\varphi(5 + 0.1(-\sin(15\varphi)\sin(2x+y) + \cos(15\phi)\sin(1x-2y))) \\
& + \cos\varphi(8 + 0.1(\cos(37\varphi)\sin(6x+7y) - \sin(37\varphi)\sin(7x-6y))) \\
\dot{\varphi} =& 1 + 0.1\cos(34\phi)(\cos(7x+6y) - \cos(6x-7y)),
\end{aligned} \tag{5.0.4}$$

with initial values $x(0) = 5$, $y(0) = 3$, $\varphi(0) = 2$. The solution to this system has a much greater radius of rotation and we can clearly see it on the figure 5.4. The result is that the solution loops around the boundary of the unit square, as in the solution in figure 5.2, but more than two times per orbit. This does not seem to affect the solution greatly because, as in the previous example, the trajectory seems very close to being circular.

As expected by our earlier results, the orbits follow a roughly circular motion similar to the motion of the unperturbed system. This circular shape is slightly distorted by the effect of the perturbation.

We have also stated several results on the stability of such orbits. To observe these in numerical examples, we need to compute a Poincaré map of our system. We chose our crossing surface to be $\varphi = 0$ because it also is at that surface that we need to move points that "escape" our torus. Since we work with a sample of points, there will never be a point situated exactly on the surface so we have to make a linear estimation of the map using the points immediately before and after the crossing. The following figure 5.5 shows the estimation of the Poincaré map for the system

$$\begin{aligned}
\dot{x} =& \cos(\varphi)(v_x + \varepsilon(\sin(5\varphi)\sin(x+y) + \cos(5\varphi)\sin(x-y))) \\
& - \sin(\varphi)(v_y + \varepsilon(\cos(2\varphi)(\cos(2x+3y) - \cos(3x-2y)))) \\
\dot{y} =& \cos(\varphi)(v_y + \varepsilon(\cos(2\varphi)(\cos(2x+3y) - \cos(3x-2y)))) \\
& + \sin(\varphi)(v_x + \varepsilon(\sin(5\varphi)\sin(x+y) + \cos(5\varphi)\sin(x-y)))
\end{aligned} \tag{5.0.5}$$

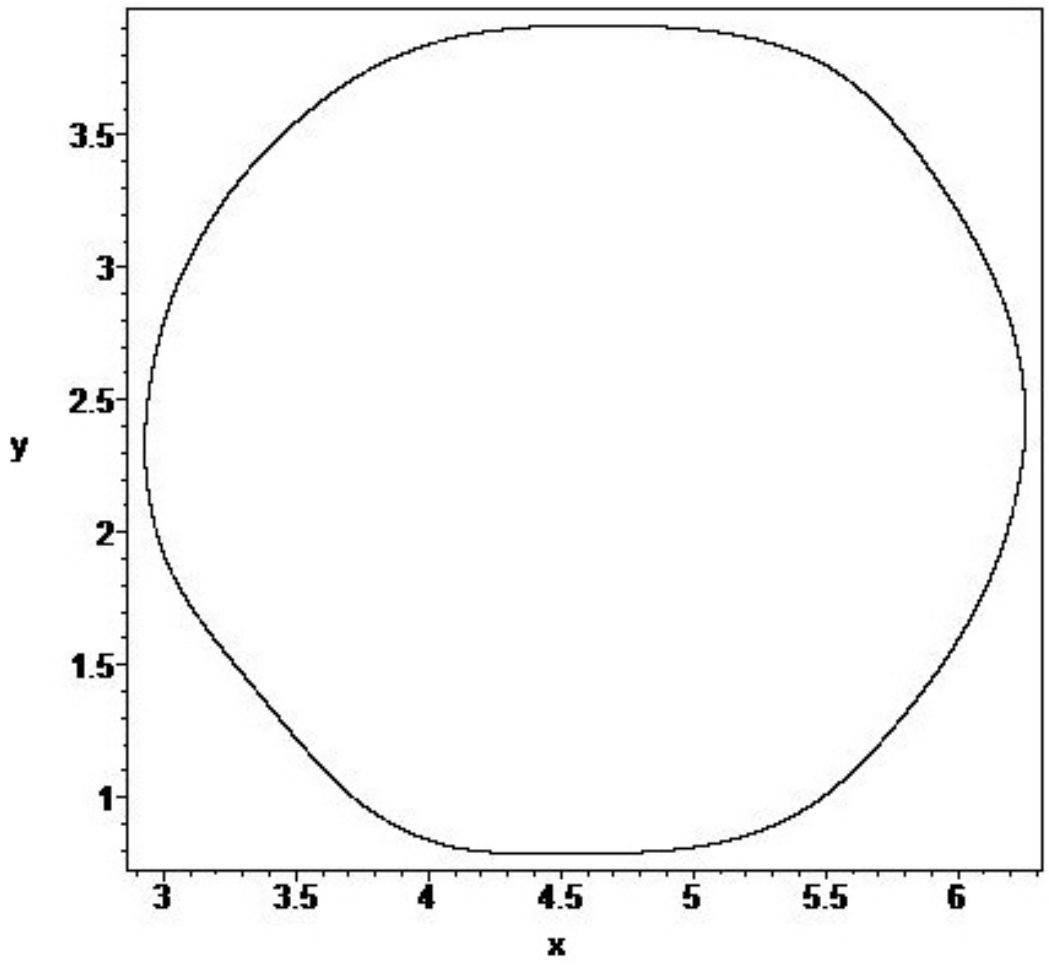

Figure 5.1: Projection on the xy plane of the simulation of the system (5.0.2).

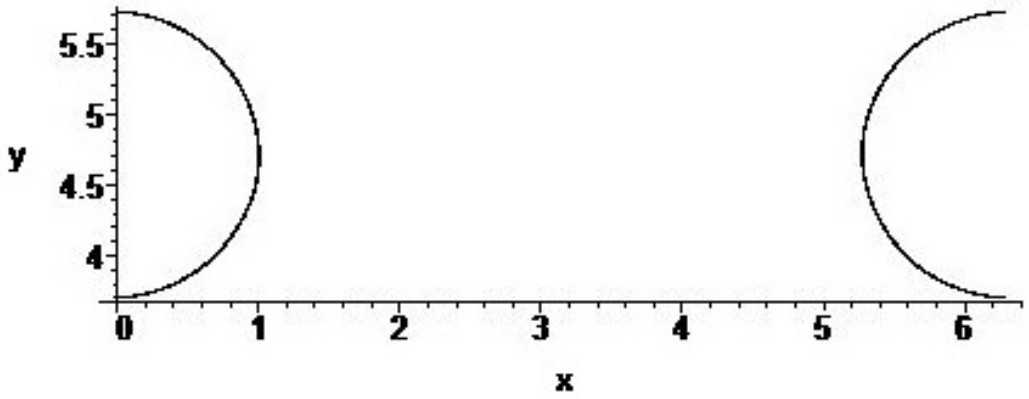

Figure 5.2: Projection on the xy plane of the simulation of the system (5.0.3).

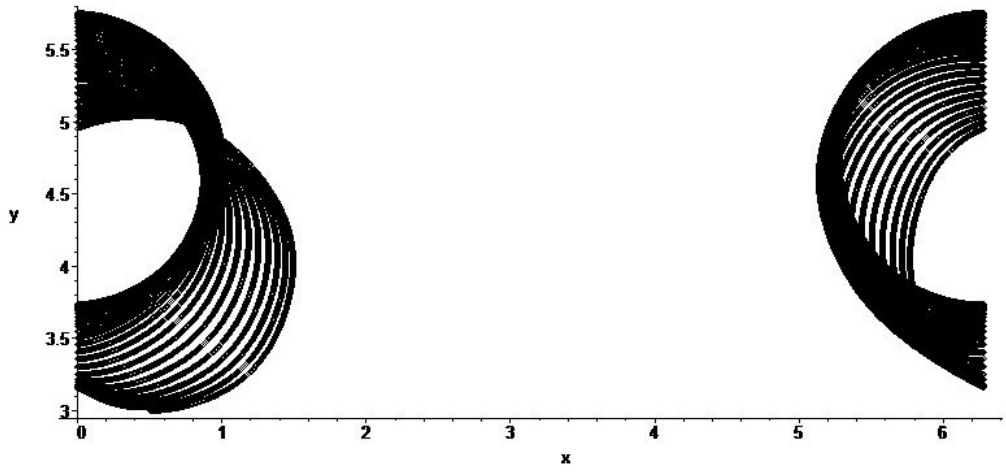

Figure 5.3: Projection on the xy plane of the simulation of the system (5.0.3) with transient phase.

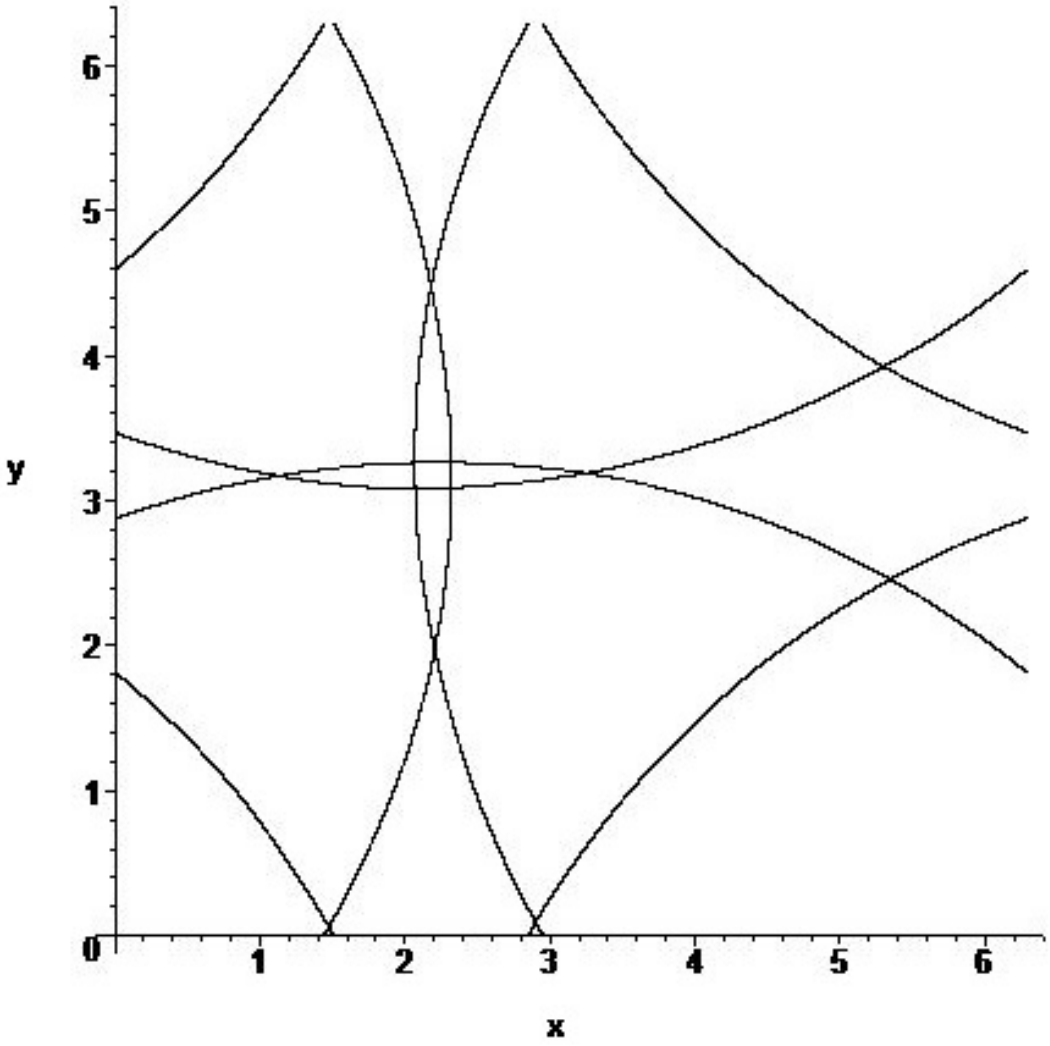

Figure 5.4: Projection of the simulation of the system (5.0.4).

$$\dot{\varphi} = \omega + \varepsilon(\sin(12\varphi)(\cos(7x + 5y) + \cos(5x - 7y))),$$

with $\varepsilon = 0.05$, $v_x = v_y = \omega = 1$. Figure 5.5 plots the results of the map for three nearby initial values. This shows that the stable orbits are indeed isolated, asymptotically stable or unstable and not part of a center. Figure 5.6 illustrates the Poincaré map of a family of stable orbits as per theorem 4.1.1. In order to get a collection of points near the fixed point of the map, we took, as a initial point the final point of the green point in figure 5.5(the set of points with initial value near (0.5, 0.5)), let's call it (x_p, y_p), and the other points are from the Poincaré map using initial conditions $Q^{-1}(e^{i\frac{n\pi}{2}}Q(x_p, y_p))$ for $n = 1, 2, 3$ as in theorem 4.1.1.

Moreover, we discovered previously that the solution with a center of rotation at the origin will have a $\frac{\pi}{2}$ spatio-temporal rotation symmetry. We computed such a solution. Figures 5.7 and 5.8 shows such a solution in the xy-plane as seen in the torus and in $\mathbb{R}^2$ respectively. We can clearly see the symmetry, especially in the latter figure.

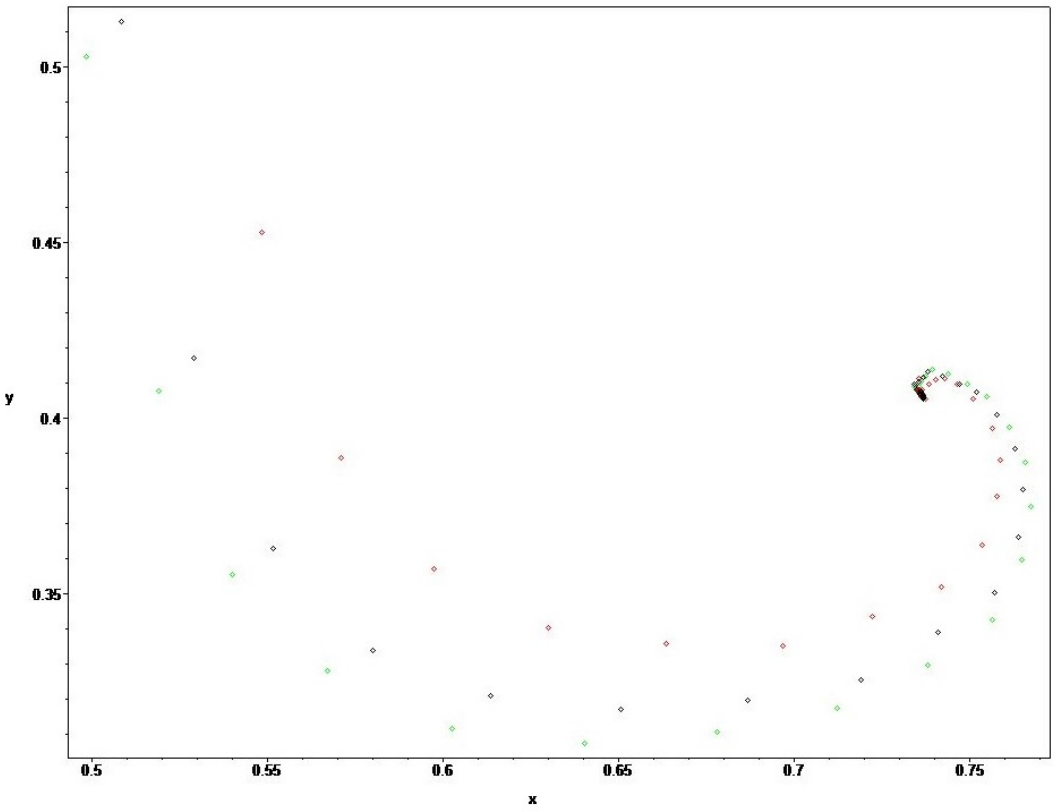

Figure 5.5: Poincare maps of the system (5.0.5) for three different initial conditions.

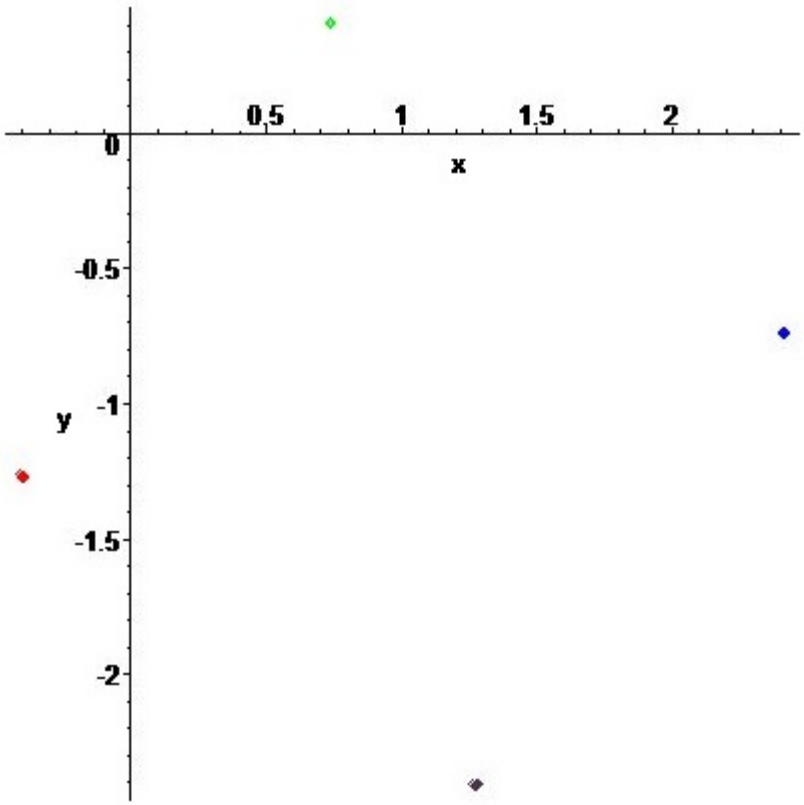

Figure 5.6: Poincare maps of a family of four solution generated by $\frac{\pi}{2}$ rotations. The initial system used was (5.0.5).

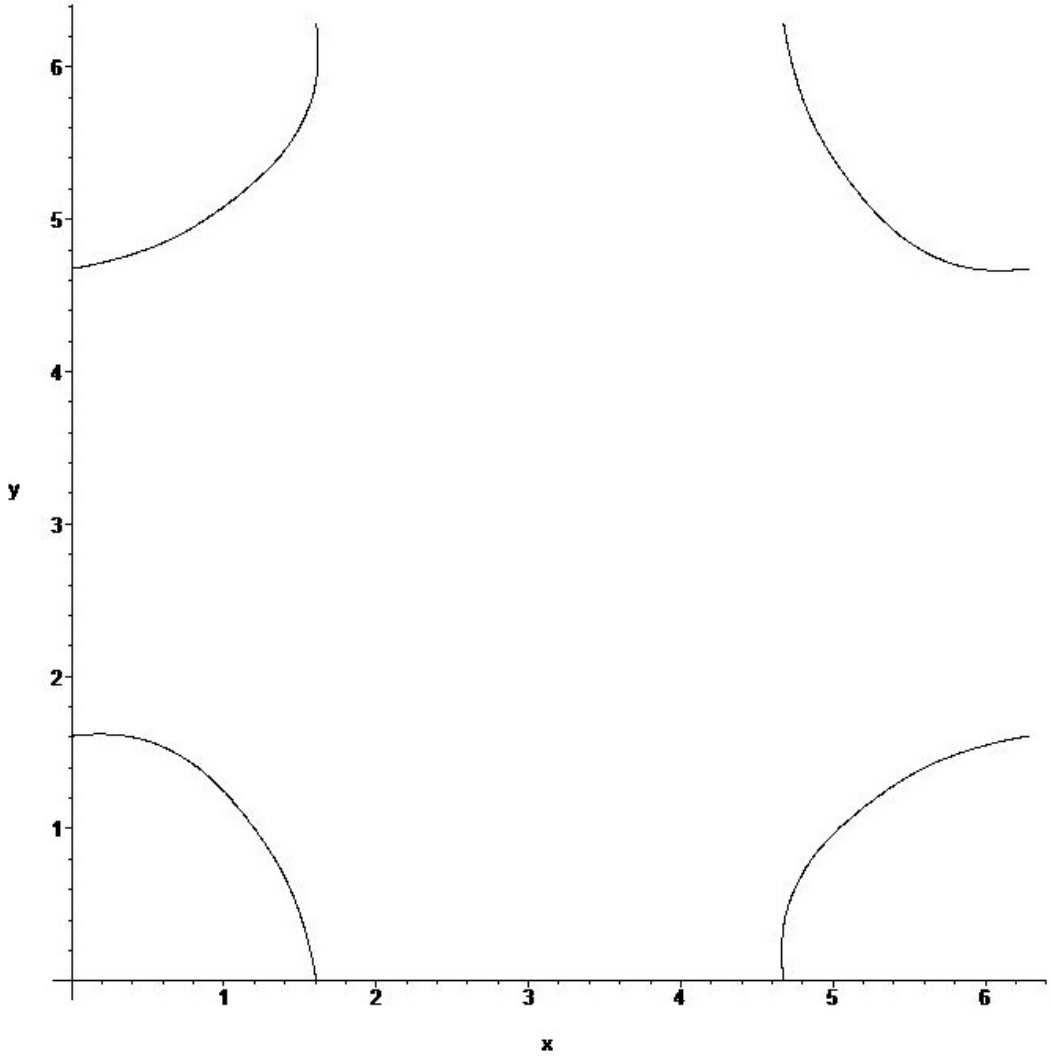

Figure 5.7: Projection in the xy-plane of a symmetric stable orbit as seen in the torus.

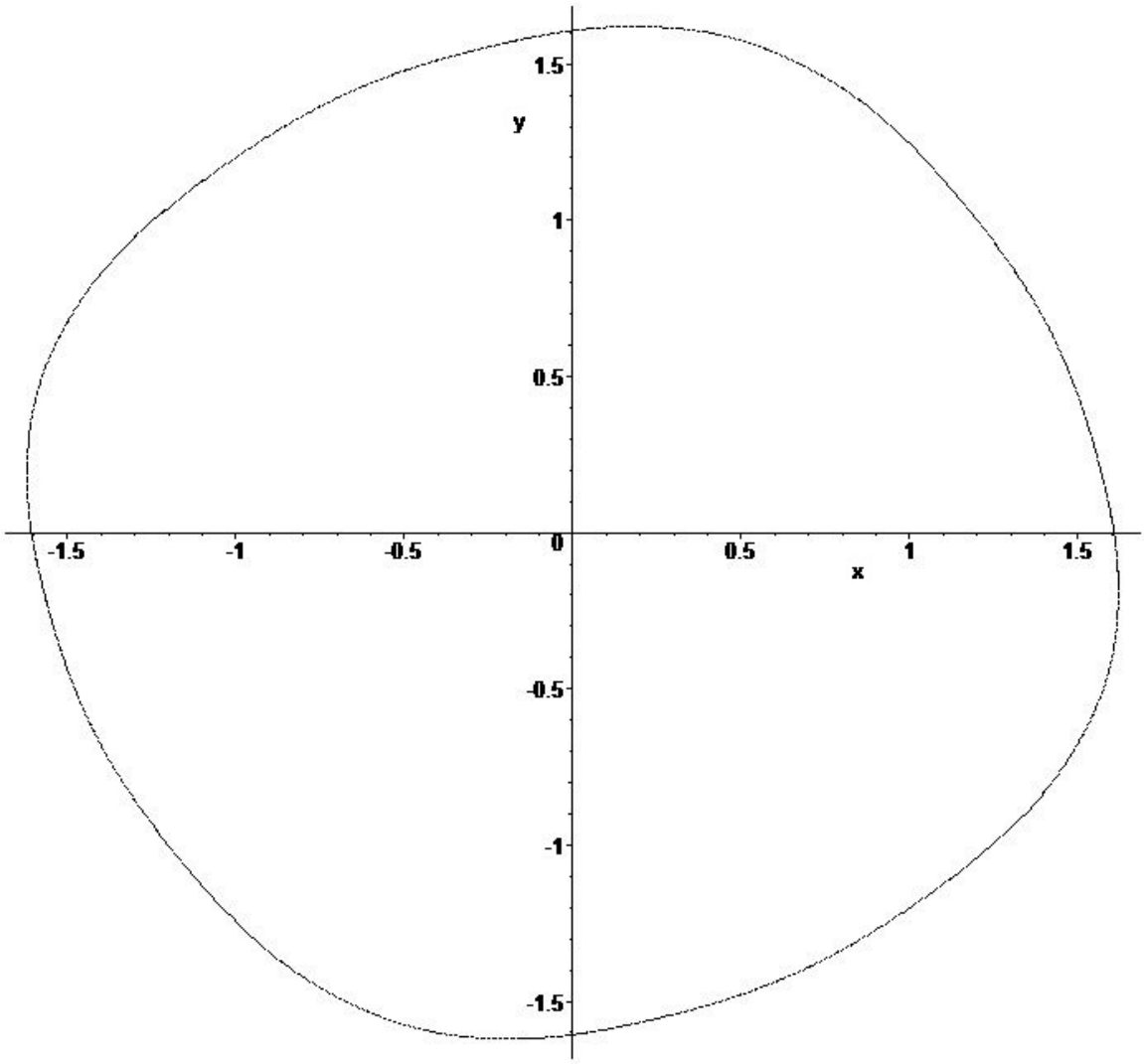

Figure 5.8: Projection in the xy-plane of a symmetric stable orbit as seen naturally in $\mathbb{R}^2$. Rotation of this solution by $\frac{\pi}{2}$ around the origin in the same as letting the system evolve by a quater of its period.

Chapter 6

Perturbed Travelling Waves

Now we bring our attention to the case of linear travelling waves, that is when $\omega = 0$ in (3.0.1). In this situation, we do not expect to observe periodic solutions because the angle φ will not change appreciably. In fact, we will show that φ oscillates about a constant value φ_0 after a transient state. In the three-torus on which we observe our solutions, it will continuously loop around in the xy coordinates and if $\frac{\operatorname{Im} e^{i\varphi_0} v}{\operatorname{Re} e^{i\varphi_0} v}$ is irrational, which is true generically, the solution will no longer be periodic; it will be dense instead. When v and φ_0 are such that $\frac{\operatorname{Im} e^{i\varphi_0} v}{\operatorname{Re} e^{i\varphi_0} v}$ is irrational, we then simply say that $ve^{i\varphi_0}$ is *irrational* (conversely we say that $ve^{i\varphi_0}$ is *rational* if the quotient is rational.

First, we consider the purely Euclidian version ($\varepsilon = 0$) of the system (3.0.1):

$$\begin{aligned} \dot{x} &= v_x \cos\varphi_0 - v_y \sin\varphi_0 \\ \dot{y} &= v_y \cos\varphi_0 + v_x \sin\varphi_0 \\ \dot{\varphi} &= 0, \end{aligned} \tag{6.0.1}$$

we can easily find that all solutions will be a line with constant φ and a slope given by $\frac{\operatorname{Im} e^{i\varphi_0} v}{\operatorname{Re} e^{i\varphi_0} v}$ in the xy projection. On the torus, the solution will either be a periodic line if $ve^{i\varphi_0}$ is rational or, otherwise, a line that will densely fill a flat horizontal surface if we assign the φ coordinate to be vertical, as in figure 6.1.

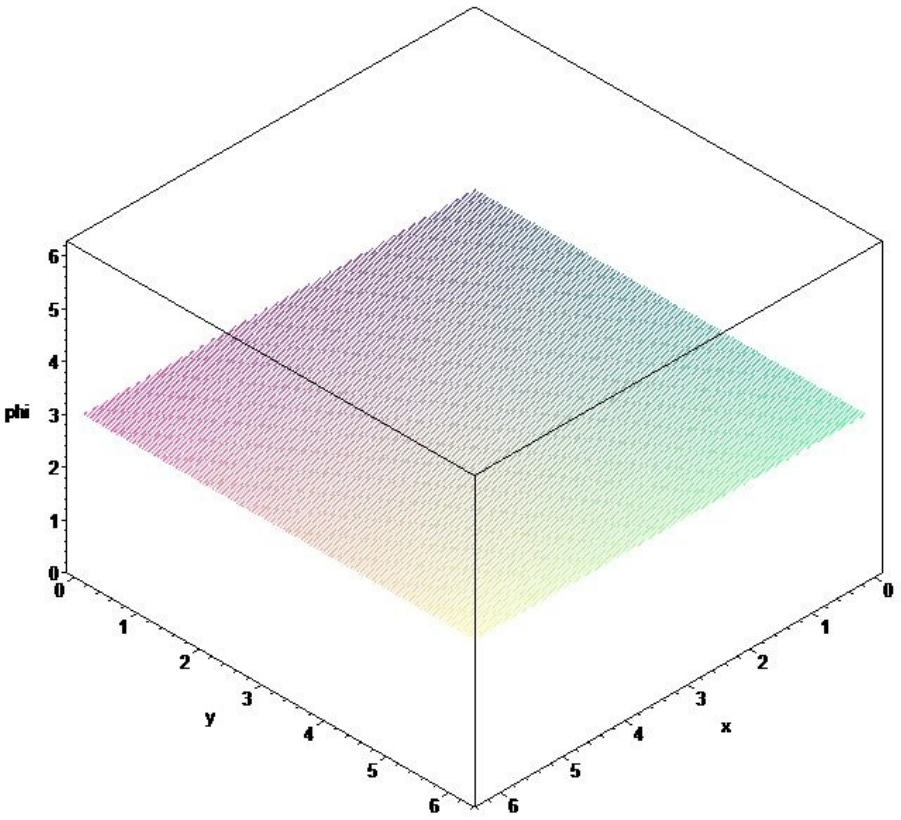

Figure 6.1: Solution of the system of differential equations (6.0.1) with initial conditions $x(0) = 1/2$, $y(0) = 1$, $\varphi(0) = 3$ in the torus

To illustrate this, we ran simulations for the following system

$$\begin{aligned} \dot{x} &= \cos\varphi - 4\sin\varphi \\ \dot{y} &= 4\cos\varphi + \sin\varphi \\ \dot{\varphi} &= 0, \end{aligned} \tag{6.0.2}$$

which corresponds to our Euclidian system (6.0.1) with initial values $x(0) = 1/2$, $y(0) = 1$, $\varphi(0) = 3$. The solution in the torus is illustrated by figure 6.1, which is a curve densely filling the surface $\varphi = 3$. However, if we change the initial value

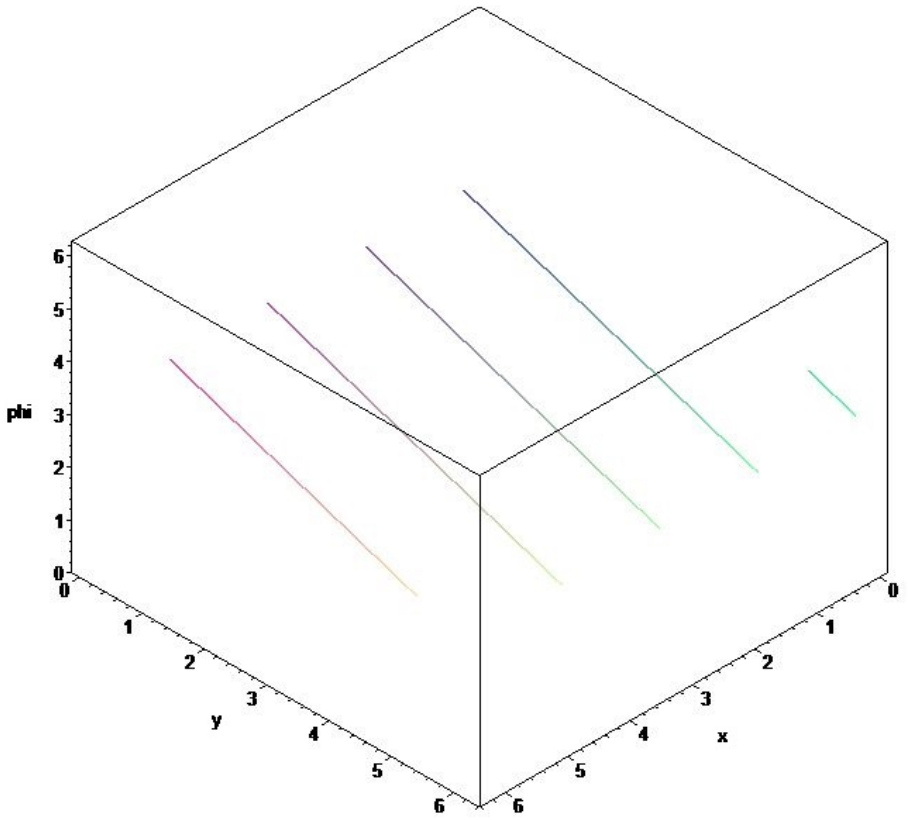

Figure 6.2: Solution of the system of differential equations (6.0.1) with initial conditions $x(0) = 1/2$, $y(0) = 1$, $\varphi(0) = \pi$ in the torus

of (6.0.2) for φ to π, $ve^{i\varphi_0} = -1 - 4i$ becomes rational and we obtain the periodic solution illustrated in figures 6.2 and 6.3. So for $\varepsilon = 0$, the solution on the three-torus is as follows. All planes of the form $\varphi = \varphi_0$ are flow-invariant and on such surfaces, the solution is periodic if $ve^{i\varphi_0}$ is rational or dense if it is irrational.

Now if we include perturbation terms in our equations, our intuition and experience from the case when $\omega \neq 0$ leads us to think that only certain invariant surfaces will survive the perturbation and will either be stable or unstable. Solutions will then be attracted to (or repelled by) such surfaces.

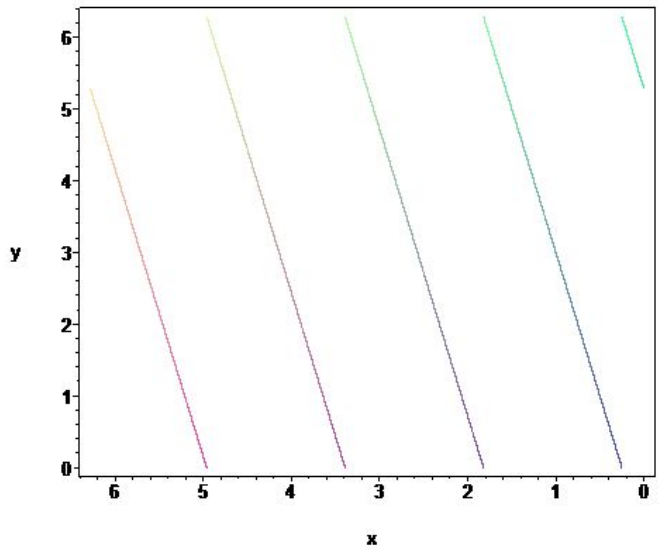

Figure 6.3: Projection of the solution of figure 6.2 in the xy plane

Theorem 6.0.1. *Let the following system of ordinary differential equations*

$$\begin{aligned}
\dot{x} &= \cos(\varphi)(v_x + \varepsilon F_x(x, y, \varphi, \varepsilon)) - \sin(\varphi)(v_y + \varepsilon F_y(x, y, \varphi, \varepsilon)) \\
\dot{y} &= \sin(\varphi)(v_x + \varepsilon F_x(x, y, \varphi, \varepsilon)) + \cos(\varphi)(v_y + \varepsilon F_y(x, y, \varphi, \varepsilon)) \\
\dot{\varphi} &= \varepsilon G(x, y, \varphi, \varepsilon),
\end{aligned} \tag{6.0.3}$$

with v_x, v_y real constants, ε near zero and G, F_x, F_y 2π-periodic functions in x, y and φ smooth enough for our purposes with Fourier coefficients corresponding to a linear combination of the eight invariant families of perturbations given in chapter 3.

Define

$$\mathcal{M}(\varphi) = \frac{1}{4\pi^2} \iint_{T^2} G(x, y, \varphi, 0) dx dy$$

and suppose that φ_0 *is such that*

i. $\mathcal{M}(\varphi_0) = 0$,

ii. $\mu = \mathcal{M}'(\varphi_0) \neq 0$.

Further suppose that the complex number $\alpha + i\beta = e^{i\varphi_o}(v_x + iv_y)$, $\alpha, \beta \in \mathbb{R}$ *is such that the Diophantine condition*

$$|n_1\alpha + n_2\beta| \geq \frac{K}{(|n_1| + |n_2|)^{\sigma+2}}, \quad \forall (n_1, n_2) \in \mathbb{Z}^2 \backslash \{(0,0)\}$$

is satisfied for some real constants $\sigma > 0$, $K > 0$. *Then for all* $\varepsilon > 0$ *small enough, (6.0.3) admits an invariant surface* $\varphi = \varphi(x, y, \varepsilon)$ *with* $\varphi(x, y, 0) \equiv \varphi_0$. *Furthermore this surface is asymptotically stable if* $\mu < 0$ *and unstable if* $\mu > 0$.

The method we shall use to prove the existence on the surfaces is the theorem 2.3 in section VII.2 of [9] stated in an appendix. In order to use this theorem we need to adapt our equations such that it corresponds to its requirements. In order to do this, we shall need some concepts from averaging theory.

6.1 Method of Averaging

Before going through our proof of the existence of the invariant surface, we will introduce the method of periodic averaging. This common method in periodic dynamical systems consists of observing the average of a rapidly oscillating function in order to look at its more general dynamics. Many references in dynamical systems or differential equations include a chapter or a section on averaging. The method stated here refers to the method of chapter 2 in [19].

We will begin this introduction with an example of the following system:

$$\begin{aligned} \dot{x} &= -x + 0.5\cos(10\ \theta), \quad x(0) = 1 \\ \dot{\theta} &= 1, \quad \theta(0) = 0. \end{aligned} \tag{6.1.1}$$

This system is very simple and can be integrated exactly by substituing θ with time t. The graph of the solution is the red oscillating curve in figure 6.4. We can see that the solution is rapidly oscillating, but gradually moves to a position where its average becomes zero. This average motion is usually more interesting than the actual motion. In our example, even if there is no equilibrium point in the system, we can clearly see that the solution is attracted to a specific form, in our case a sine type function around 0.

A closer look at the $\dot{x}$ formula in (6.1.1) reveals that there is a term which is periodic in θ, thus periodic in time with period $\frac{2\pi}{10}$. Moreover, the average of this term over its period is zero. If we consider the averaged function

$$\dot{y} = \frac{1}{2\pi}\int_0^{2\pi} -y + 0.5\cos(10s)ds = -y, \tag{6.1.2}$$

we can see that its solution follows the center of oscillation of the solution of the original system. In our example, the solution of the averaged equation (6.1.2) is represented in the black dashed line in figure 6.4

Consider the following differential equation:

$$\dot{X} = \varepsilon \mathbf{f}^1(X,t) + \varepsilon^2 \mathbf{f}^{[2]}(X,t,\varepsilon), \quad X(0) = A,$$

with $X \in \mathbb{R}^n$, $t \in \mathbb{R}$, A is a constant vector in $\mathbb{R}^n$, $\mathbf{f}^1$ and $\mathbf{f}^{[2]}$ are periodic in t with period 2π, without loss of generality. As before, we will truncate the equation and only keep the terms in ε, but we will also be averaging the equation which amounts to consider what is called the averaged equation:

$$\dot{Z} = \varepsilon \bar{\mathbf{f}}^1(Z), \quad Z(0) = A,$$

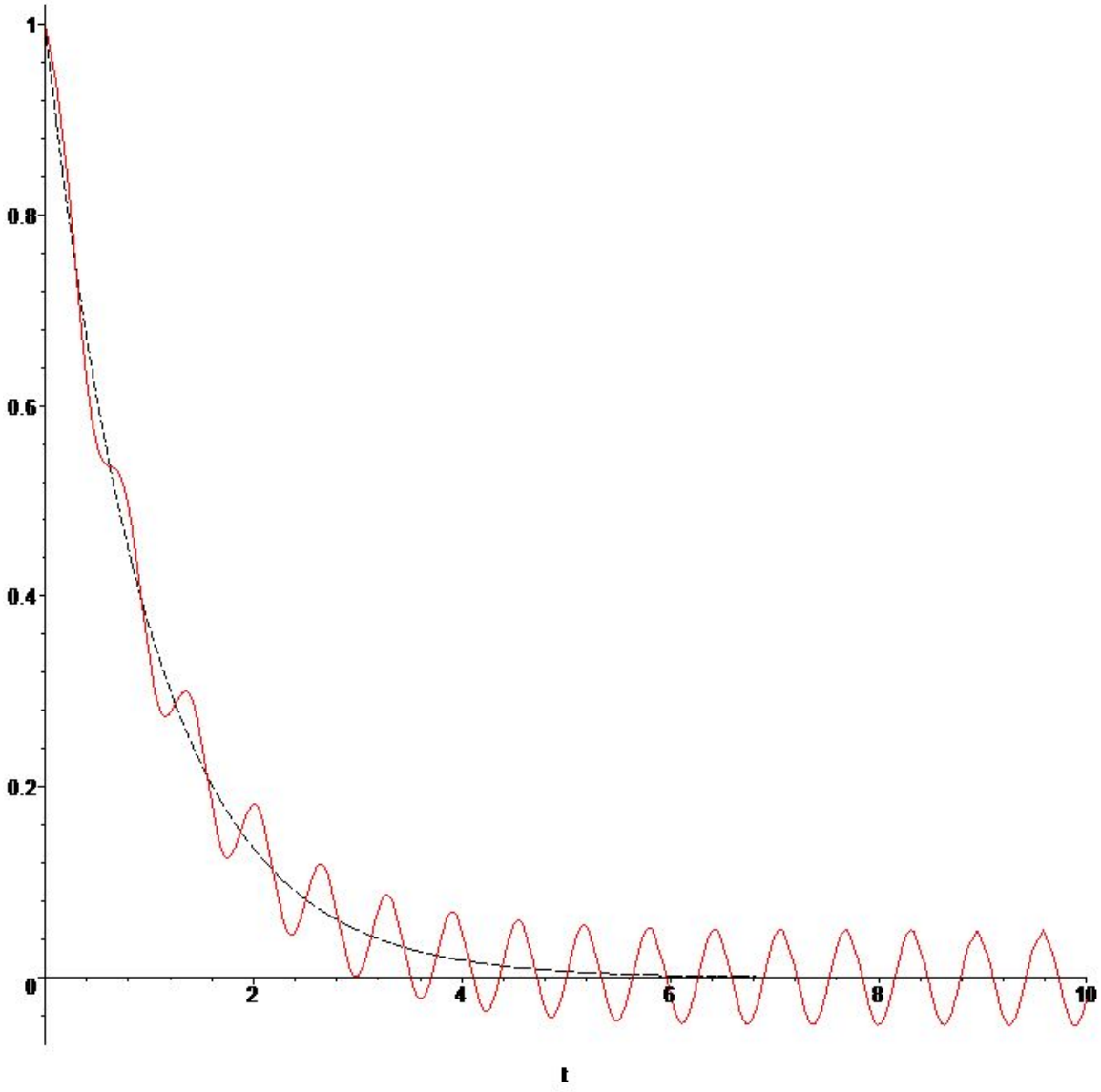

Figure 6.4: Solutions of the system (6.1.1) (in red line) and the averaged system (6.1.2) (in black).

with $\bar{\mathbf{f}}^1(Z) = \frac{1}{2\pi}\int_0^{2\pi} \mathbf{f}^1(Z,s)ds$. The main result of this method is that the solutions of the original and averaged equations stay close together for an interval of t of order $\frac{1}{\varepsilon}$. More specifically:

$$\|X(t) - Z(t)\| \leq c\,\varepsilon \text{ for } 0 \leq t \leq \frac{L}{\varepsilon},$$

where c and L are real, positive constants.

This represents the simplest form of averaging, over one variable t. In our case, we will want to average functions of the form $G(x, y, \varphi, \varepsilon)$ which is periodic in both x and y. Consider the following system of equations:

$$\begin{aligned}\dot{x} &= a + \varepsilon F_x(x, y, \varphi, \varepsilon)\\ \dot{y} &= b + \varepsilon F_y(x, y, \varphi, \varepsilon)\\ \dot{\varphi} &= \varepsilon G(x, y, \varphi, \varepsilon),\end{aligned}$$

with a and b constants which are not both zero, G, F_x and F_y are all 2π-periodic in both x and y. Suppose also without loss of generality that the average

$$\overline{F}(\varphi, \varepsilon) = \frac{1}{4\pi^2}\int_{T^2} F_{x,y}(x, y, \varphi, \varepsilon)dxdy = 0,$$

with T^2 representing the torus containing one period of $F_{x,y}$ in the x and y direction. Under certain conditions, we can use the method of averaging to simplify the $\dot{\varphi}$ equation to

$$\dot{\bar{\varphi}} = \varepsilon\bar{G}(\varphi, \varepsilon) = \frac{1}{4\pi^2}\int_{T^2} G(x, y, \varphi, \varepsilon)dxdy,$$

with the bar representing the average over x and y. Throughout this chapter, when averaging is used on an equation, it will be assumed that this manoeuvre was used and we drop the bar.

6.2 Proof of Existence of an Invariant Surface

We have the following system of equations:

$$\dot{x} = \cos(\varphi)(v_x + \varepsilon F_x(x, y, \varphi, \varepsilon)) - \sin(\varphi)(v_y + \varepsilon F_y(x, y, \varphi, \varepsilon))$$

$$\dot{y} = \sin(\varphi)(v_x + \varepsilon F_x(x, y, \varphi, \varepsilon)) + \cos(\varphi)(v_y + \varepsilon F_y(x, y, \varphi, \varepsilon))$$
$$\dot{\varphi} = \varepsilon G(x, y, \varphi, \varepsilon).$$

Expand the Taylor series of G on ε near zero:

$$\dot{\varphi} = \varepsilon G^0(x, y, \varphi) + \varepsilon^2 G^1(x, y, \varphi) + \cdots .$$

apply the substitution $\varphi = \varphi_0 + \varepsilon^{\frac{1}{2}}\hat{\varphi}$, then calculate the Taylor coefficients again on ε near zero:

$$\dot{\varphi} = \varepsilon^{\frac{1}{2}} G_0^0(x, y) + \varepsilon\varphi G_1^0(x, y) + \varepsilon^{\frac{3}{2}}(G_0^1(x, y) + \frac{1}{2}\varphi^2 G_2^0(x, y)) + \frac{1}{2}\varepsilon^2\varphi G_1^1(x, y) + O(\varepsilon^{\frac{5}{2}}),$$

where the superscripts on the G terms represent the order of the derivative of G with respect to ε at $\varepsilon = 0$ and the number in subscript the order of the derivative with respect to φ at $\varphi = \varphi_0$. Each time such a substitution will be made, we will drop the hat notation as we apply it.

Applying this substitution to $\dot{x}$ gives:

$$\begin{aligned}
\dot{x} =& \cos(\varphi_0 + \varepsilon^{\frac{1}{2}}\varphi)(v_x + \varepsilon F_x(x, y, \varphi, \varepsilon)) - \sin(\varphi_0 + \varepsilon^{\frac{1}{2}}\varphi)(v_y + \varepsilon F_y(x, y, \varphi, \varepsilon)) \\
=& (\cos\varphi_0 - \varepsilon^{\frac{1}{2}}\varphi\sin\varphi_0 + \cdots)(v_x + \varepsilon F_x(x, y, \varphi, \varepsilon)) \\
& - (\sin\varphi_0 + \varepsilon^{\frac{1}{2}}\varphi\cos\varphi_0 + \cdots)(v_y + \varepsilon F_y(x, y, \varphi, \varepsilon)) \\
=& (v_x\cos\varphi_0 - v_y\sin\varphi_0) + \varepsilon^{\frac{1}{2}}(-v_x\varphi\sin\varphi_0 - v_y\varphi\cos\varphi_0) + \varepsilon(\cos\varphi_0 F_x(x, y, \varphi_0, 0) \\
& - \sin\varphi_0 F_y(x, y, \varphi_0, 0) - \frac{v_x\varphi^2}{2}\cos\varphi_0 + \frac{v_y\varphi^2}{2}\sin\varphi_0) + O(\varepsilon^{\frac{3}{2}})
\end{aligned}$$

Similarly, $\dot{y}$ becomes

$$\begin{aligned}
\dot{y} =& (v_x\sin\varphi_0 + v_y\cos\varphi_0) + \varepsilon^{\frac{1}{2}}(v_x\varphi\cos\varphi_0 - v_y\varphi\sin\varphi_0) \\
& + \varepsilon(\sin\varphi_0 F_x(x, y, \varphi_0, 0) + \cos\varphi_0 F_y(x, y, \varphi_0, 0) + \frac{v_x\varphi^2}{2}\sin\varphi_0 - \frac{v_y\varphi^2}{2}\cos\varphi_0) \\
& + O(\varepsilon^{\frac{3}{2}}).
\end{aligned}$$

To simplify the notation, we shall now work in vector form, with

$$X := \begin{pmatrix} x \\ y \end{pmatrix}, \quad V := \begin{pmatrix} v_x \\ v_y \end{pmatrix}, \quad R_\varphi = \begin{pmatrix} \cos\varphi & -\sin\varphi \\ \sin\varphi & \cos\varphi \end{pmatrix}.$$

We then obtain the formula

$$\dot{X} = R_{\varphi_o} V + \varepsilon^{\frac{1}{2}} R'_{\varphi_o} V\varphi + \varepsilon[R_{\varphi_0} F(X, \varphi_0, 0) + \frac{1}{2} R''_{\varphi_o} V\varphi^2] + O(\varepsilon^{\frac{3}{2}})$$

We now introduce the change of variable $\varphi = \hat{\varphi} + \varepsilon^{\frac{1}{2}} Y(X)$, which leads to

$$\begin{aligned}
\dot{X} =& R_{\varphi_o} V + \varepsilon^{\frac{1}{2}} R'_{\varphi_o} V\varphi + \varepsilon[R_{\varphi_o} F(X, \varphi_0, 0) + \frac{1}{2} R''_{\varphi_o} V\varphi^2 + R'_{\varphi_o} VY(X)] + O(\varepsilon^{\frac{3}{2}}) \\
\dot{\varphi} =& \varepsilon[G_1^0(X) - D_X Y(X) R'_{\varphi_o} V]\varphi + \varepsilon^{\frac{3}{2}}[G_0^1(X) + \frac{1}{2}\varphi^2 G_2^0(X) + G_1^0 Y(X) \\
& - D_X Y(X)(R'_{\varphi_o} VY(X) + R_{\varphi_o} F(X, \varphi_0, 0) + \frac{1}{2} R''_{\varphi_o} V\varphi^2)] + O(\varepsilon^2).
\end{aligned}$$

Such a formulation exists if Y satisfies the following partial differential equation:

$$D_X Y(X) R_{\varphi_o} V = G_0^0(X). \tag{6.2.1}$$

We will now prove this previous statement:

Proof: Following the change of variables, the equation for $\dot{\varphi}$ becomes

$$\dot{\varphi} = \dot{\hat{\varphi}} + \varepsilon^{\frac{1}{2}} D_X Y(X)\dot{X}.$$

Isolating $\dot{\hat{\varphi}}$ and expanding the known derivatives yields

$$\begin{aligned}
\dot{\varphi} =& \varepsilon^{\frac{1}{2}} G_0^0(X) + \varepsilon(\varphi + \varepsilon^{\frac{1}{2}} Y(X)) G_1^0(X) + \varepsilon^{\frac{3}{2}}[G_0^1(X) + \frac{1}{2}(\varphi + \varepsilon^{\frac{1}{2}} Y(X))^2 G_2^0(X)] \\
& - \varepsilon^{\frac{1}{2}} D_X Y(X)[R_{\varphi_o} V + \varepsilon^{\frac{1}{2}} R'_{\varphi_o} V(\varphi + \varepsilon^{\frac{1}{2}} Y(X)) + \varepsilon[R_{\varphi_o} F(X, \varphi_0, 0) \\
& + \frac{1}{2} R''_{\varphi_o} V(\varphi + \varepsilon^{\frac{1}{2}} Y(X))^2]] + O(\varepsilon^2) \\
=& \varepsilon^{\frac{1}{2}}[G_0^0(X) - D_X Y(X) R_{\varphi_o} V] + \varepsilon[\varphi G_1^0(X) - D_X Y(X) R'_{\varphi_o} V\varphi] + \varepsilon^{\frac{3}{2}}[G_0^1(X) \\
& + \frac{1}{2}\varphi^2 G_2^0(X) + G_1^0 Y(X) - D_X Y(X)(R'_{\varphi_o} VY(X) + R_{\varphi_o} F(X, \varphi_0, 0) \\
& + \frac{1}{2} R''_{\varphi_o} V\varphi^2)] + O(\varepsilon^2)
\end{aligned}$$

Thus, if $Y(X)$ satisfies the equation (6.2.1), the first term in the differential equation vanishes and we get what we want. Since (6.2.1) is a non-homogeneous transport equation, there will exist a suitable $Y(X)$ because our choice of $G_0^0(X) = G(X, \varphi_0, 0)$ is smooth enough. ∎

We can write the formal solution of $Y(X)$ of (6.2.1) in the form of a Fourier series.

$$Y(x, y, \hat{\varphi}) = \sum_{\nu \neq 0} \frac{a_\nu^1(\hat{\varphi})}{i\nu \cdot R_{\varphi_o} V} e^{i(\nu_1 x + \nu_2 y)} \ , \tag{6.2.2}$$

with ν, a two-dimensional integer vector and a^1, the first term in the ε expansion of the Fourier series of the right hand side of the previous equation (6.2.1). Since $R_{\varphi_o} V$ is irrational, the denominator in the solution is never zero, but it can be arbitrarily small, which means that the series may not converge. We call this problem the small divisor problem. To guarantee the convergence of our solution, we need additional hypotheses. We may assume that the sum is finite or that there is a bound on the denominator, that is there exists constants $\alpha > 0$, $\gamma > 0$ such that

$$|\nu \cdot V| \geq \frac{\gamma}{|\nu|^{\alpha+2}}. \tag{6.2.3}$$

Conditions such as this are commonplace in problems involving averaging. A series with denominators satisfying this condition are said to be badly incommensurable, and one can show that it converges [1].

Continuing with our work, use another substitution $\varphi = \varepsilon^{\frac{1}{2}} \hat{\varphi}$ to get

$$\begin{aligned}
\dot{X} =& R_{\varphi_0} V + \varepsilon R'_{\varphi_0} V \varphi + \varepsilon [R_{\varphi_0} F(X, \varphi_0, 0) + R'_{\varphi_0} V Y(X)] + O(\varepsilon^{\frac{3}{2}}) \\
\dot{\varphi} =& \varepsilon [G_1^0(X) - D_X Y(X) R'_{\varphi_0} V] \varphi + \varepsilon [G_0^1(X) + G_1^0(X) Y(X) \\
& - D_X Y(X)(R'_{\varphi_0} V Y(X) + R_{\varphi_0} F(X, \varphi_0, 0))] + O(\varepsilon^{\frac{3}{2}}).
\end{aligned}$$

We then apply another substitution $\varphi = \hat{\varphi} = \varepsilon[Z_1(X) + Z_2(X)\hat{\varphi}]$ such that

$$\begin{aligned} D_X Z_1 V &= G_0^1(X) + G_1^0(X)Y(X) - D_X Y(X)(R'_{\varphi_0} V Y(X) + R_{\varphi_0} F(X, \varphi_0, 0)) - \lambda_1 \\ &= A(X) - \lambda_1 \\ D_X Z_2 V &= -D_X Y(X) R'_{\varphi_0} V - \lambda_2, \end{aligned}$$

with $\lambda_1 = \frac{1}{4\pi^2} \iint\limits_{T^2} A(X)dX$, $\lambda_2 = \frac{1}{4\pi^2} \iint\limits_{T^2} -D_X Y(X) R'_{\varphi_0} V dX$. After averaging $\dot{\varphi}$ over X, we get

$$\begin{aligned} \dot{X} &= R_{\varphi_0} V + O(\varepsilon) \\ \dot{\varphi} &= \varepsilon[(\mathcal{M}'(\varphi_0) + \lambda_2)\varphi + \lambda_1] + O(\varepsilon^{\frac{3}{2}}), \end{aligned}$$

with $\mathcal{M}'(\varphi_0) = \frac{\partial}{\partial \varphi} \frac{1}{4\pi^2} \iint\limits_{T^2} G(X, \varphi, 0)dX\Big|_{\varphi=\varphi_0}$. From the Fourier series for $Y(X)$ (6.2.2), we can see that the integral on the torus T^2 of its derivatives on X are zero, therefore $\lambda_2 = 0$. Finally, the translation $\varphi = \hat{\varphi} - \frac{\lambda_1}{\mathcal{M}'(\varphi_0)}$ and the grouping of all higher order terms into the functions $\Theta_1(X, \varphi, \varepsilon)$, $\Theta_2(X, \varphi, \varepsilon)$ gives us our desired form to apply theorem A.0.1 in the annex:

$$\begin{aligned} \dot{X} &= R_{\varphi_0} V + \varepsilon \Theta_2(X, \varphi, \varepsilon) \\ \dot{\varphi} &= \varepsilon \mu \varphi + \varepsilon \Theta_1(X, \varphi, \varepsilon), \end{aligned}$$

with $\mu = \mathcal{M}'(\varphi_0)$. We need the same restrictions here for small divisors on Z_1, Z_2 as in (6.2.3). The method to find Z_1, Z_2 is very similar as in the previous proof only here we have two equations which we can separate in order to get two transport equation. We also need to add λ_1 in our formulas as the average of the functions we wish to simplify might no longer be zero, but our functions $Z_{1,2}$ need to average zero.

The physical interpretation of this result is that generically, solutions of the system (3.0.1) with $\omega = 0$ behave in a similar fashion to the solution illustrated in figure 6.4. That is, the solution goes through a transient phase after which it oscillates about a specific value of φ. Where the system in figure 6.4 oscillated as a sine function,

the perturbed travelling wave will densely trace an oscillating two-variable function in the three-torus phase space. In a physical experiment, the spiral wave will seem to move in a linear trajectory, but this motion will be slightly perturbed with oscillations. These oscillations could then be solved by finding the position of the spiral tip in the torus at any time. Moreover, we can also conclude from continuity that for values of $\omega > 0$ smaller than ε the invariant surface persists. Thus, quasi-linear drifting of the spiral wave is a stable phenomena in the phase space of (1.0.1).

Chapter 7

Example of an $\omega = 0$ system

We saw in the last section that under certain conditions an invariant surface exists for our system (3.0.1) in the case $\omega = 0$. However the methods used to prove its existence give no way to describe it. We will try to illustrate such an invariant surface in a specific example. Consider the following system:

$$\begin{aligned}
\dot{x} &= \cos(\varphi)(v_x + \varepsilon F_x(x, y, \varphi, \varepsilon)) - \sin(\varphi)(v_y + \varepsilon F_y(x, y, \varphi, \varepsilon)) \\
\dot{y} &= \sin(\varphi)(v_x + \varepsilon F_x(x, y, \varphi, \varepsilon)) + \cos(\varphi)(v_y + \varepsilon F_y(x, y, \varphi, \varepsilon)) \\
\dot{\varphi} &= \varepsilon G(x, y, \varphi, \varepsilon)
\end{aligned} \tag{7.0.1}$$

Since we are trying to characterize a surface on the system near $\dot{\varphi} = 0$, we will look to a formulation of φ as a function of x and y. Its derivative becomes

$$\dot{\varphi} = \frac{\partial \varphi}{\partial x}\dot{x} + \frac{\partial \varphi}{\partial y}\dot{y} = \varepsilon G(x, y, \varphi, \varepsilon).$$

Substituting from the original system, we get

$$\begin{aligned}
&\frac{\partial \varphi}{\partial x}(\cos(\varphi)(v_x + \varepsilon F_x(x, y, \varphi, \varepsilon)) - \sin(\varphi)(v_y + \varepsilon F_y(x, y, \varphi, \varepsilon))) \\
+&\frac{\partial \varphi}{\partial y}(\sin(\varphi)(v_x + \varepsilon F_x(x, y, \varphi, \varepsilon)) + \cos(\varphi)(v_y + \varepsilon F_y(x, y, \varphi, \varepsilon))) \\
&= \varepsilon G(x, y, \varphi, \varepsilon).
\end{aligned}$$

After taking the expansion of φ on ε near φ_0, which is the center of oscillation of the surface and the value where the average of G over x and y yields zero, as well as the expansion of G on ε and keeping the first order terms, we get

$$\begin{aligned}\frac{\partial\varphi}{\partial x}(v_x\cos(\varphi_0) - v_y\sin(\varphi_0)) + \frac{\partial\varphi}{\partial y}(v_x\sin(\varphi_0) + v_y\cos(\varphi_0))\\ =\varepsilon G(x, y, \varphi_0, 0).\end{aligned}$$

This is a nonhomogeneous transport equation and its general solution is a specific solution to the equation added with the general solution of the homogeneous equation. First let us introduce the following notation, for the sake of brevity:

$$\begin{aligned}a &:= (v_x\cos(\varphi_0) - v_y\sin(\varphi_0))\\ b &:= (v_x\sin(\varphi_0) + v_y\cos(\varphi_0))\end{aligned}$$

The general solution of the homogeneous transport equation is simply the function $f(x - \frac{a}{b}y)$, where f is differentiable. However, if we apply the periodicity conditions, no function other than 0 satisfies the homogeneous equation if $\frac{a}{b}$ is irrational. We will restrict ourselves to this case as it covers almost every case.

To find the specific solution, we use the methods of characteristics. Consider the following substitution:

$$\xi = ax + by, \quad \eta = bx - ay.$$

By applying the chain rule and substituting back we can easily demonstrate that the solution is

$$\varphi(x, y) = C(\eta) + \int \frac{G(\frac{a\xi+b\eta}{a^2+b^2}, \frac{b\xi-a\eta}{a^2+b^2}, \varphi_0, 0)}{a^2 + b^2}d\xi,$$

Where C is the integration constant. Its value will depend on φ_0 and can be quite difficult to find except in a particular case. It is when the perturbation has the form $G(x, y, \varphi, \varepsilon) = G_1(\varphi, \varepsilon) + G_2(x, y, \varepsilon)$. Here we have separated the perturbation on φ into two terms: one dependent only on φ and the other only on x and y. This will

have the effect of "locking" the surfaces near stable zeros of G_1, where the derivative $G_{1\varphi}(\varphi_0, \varepsilon) < 0$. Let's continue with a simple numerical example.

As an example consider the previous system with the following perturbation terms:

$$\begin{aligned} G_1(\varphi, \varepsilon) &= 2\sin(4\varphi) \\ G_2(x, y, \varepsilon) &= \cos(7x + 6y) + \cos(6x - 7y) \\ F_x(x, y, \varphi, \varepsilon) &= \sin(5\varphi)\sin(x + y) + \cos(5\varphi)\sin(x - y) \\ F_y(x, y, \varphi, \varepsilon) &= \cos(2\varphi)(\cos(2x + 3y) - \cos(3x - 2y)) \\ x(0) = 0.5, \quad y(0) &= 1, \quad \varphi(0) = 0.785. \end{aligned} \tag{7.0.2}$$

The parameter values are:

$$\varepsilon = 0.1, \quad v_x = \pi, \quad v_y = \sqrt{2}. \tag{7.0.3}$$

Note that here we have $G_0(x, y, \varepsilon) = G(x, y, 0) = G(x, y, \varepsilon)$.

We will look at the solution near $\varphi_0 = \frac{\pi}{4}$, which is a stable zero of G_1. The calculated surface equation from the transport equation yields

$$\varphi_c(x, y) = \frac{\pi}{4} + \varepsilon \left(2\frac{(26 + \pi\sqrt{2})\sin(7x + 6y) + (13\pi\sqrt{2} - 2)\sin(-6x + 7y)}{(13\pi\sqrt{2} - 2)(26 + \pi\sqrt{2})} \right).$$

This approximation is very close to the computed simulation. To verify this, we have simulated the system using the *dsolve* tool with the Fehlberg fourth-fifth order Runge-Kutta method in Maple. From this simulation, we take a sample of one hundred thousand and one points separated by a time increment of 0.005. Then we match the (x, y) position of each point with the value of the estimation. This way we can take the distance between the simulation and the estimation point per point. We then keep the last half of those points (fifty thousand and one) to build a plot of the difference. The next three figures represent respectively the simulation (figure 7.1), estimation (figure 7.2) and difference (figure 7.3) point plots for the system (7.0.2) with mentioned initial points.

Observing these figures, we see the close resemblance between the simulated and estimated plots. This observation is confirmed with the difference plot, which has an amplitude of superior order in ε.

Moreover, we also ran simulations and computed estimations of the system for different values of ε (7.0.2) in order to observe the behaviour of our estimated surface as ε goes to 0. According to the theorem of existence of the invariant two-torus, its non-constant terms should vanish as this limit. Figure 7.4 represent different average distance between points for these computations and we clearly see that the distance goes to zero as ε goes to zero.

It is also important to point out that the transient state has been especially removed in figure 7.1 due to its initial value in φ which is very close to the invariant surface. Figure 7.5 shows the system with a significative transient state. We can clearly see that the surface is a specific stable invariant surface, as the function quickly approaches it.

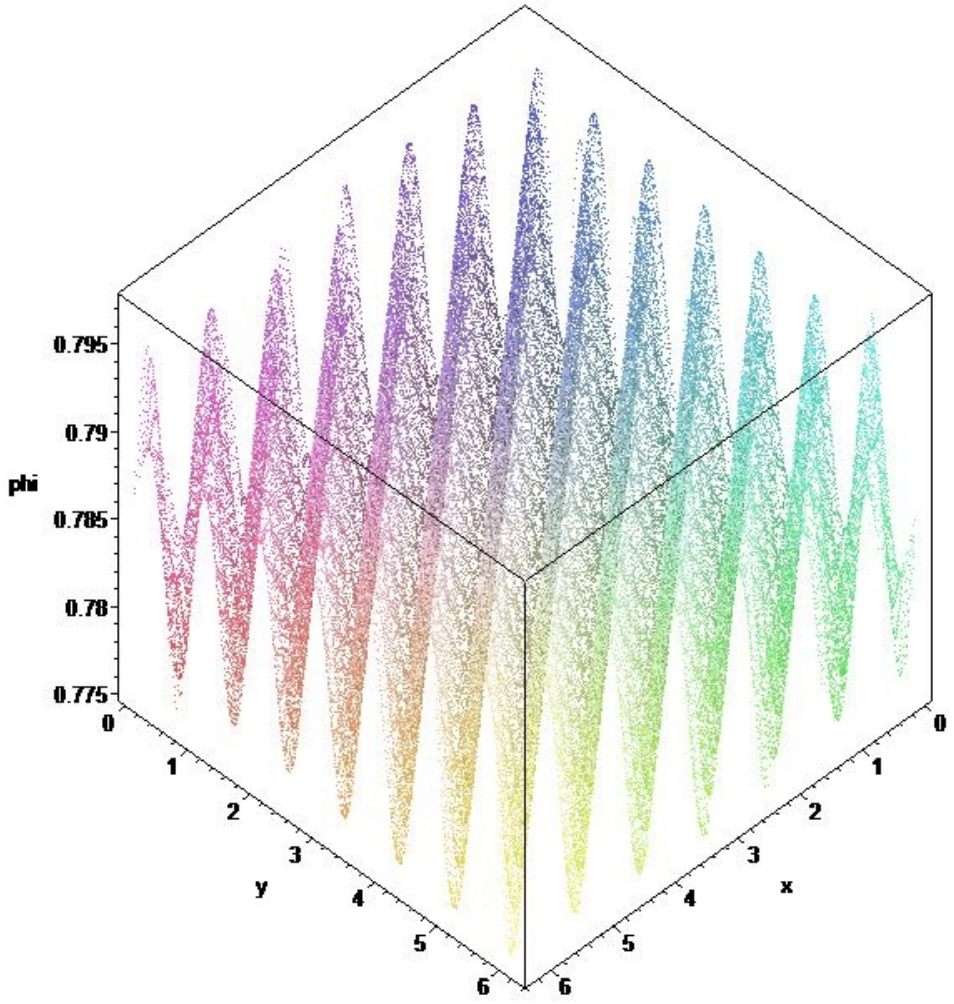

Figure 7.1: Simulation of system (7.0.2) with parameter values (7.0.3)

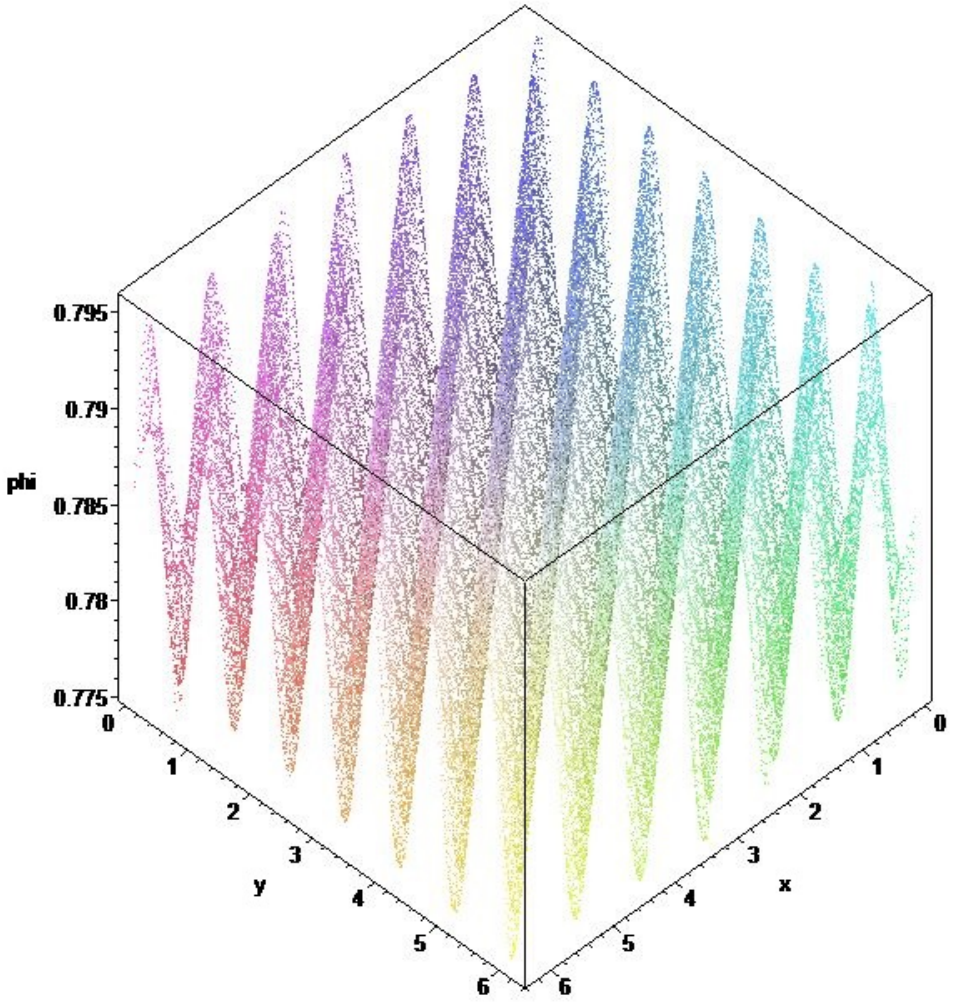

Figure 7.2: Estimation of system (7.0.2) with parameter values (7.0.3)

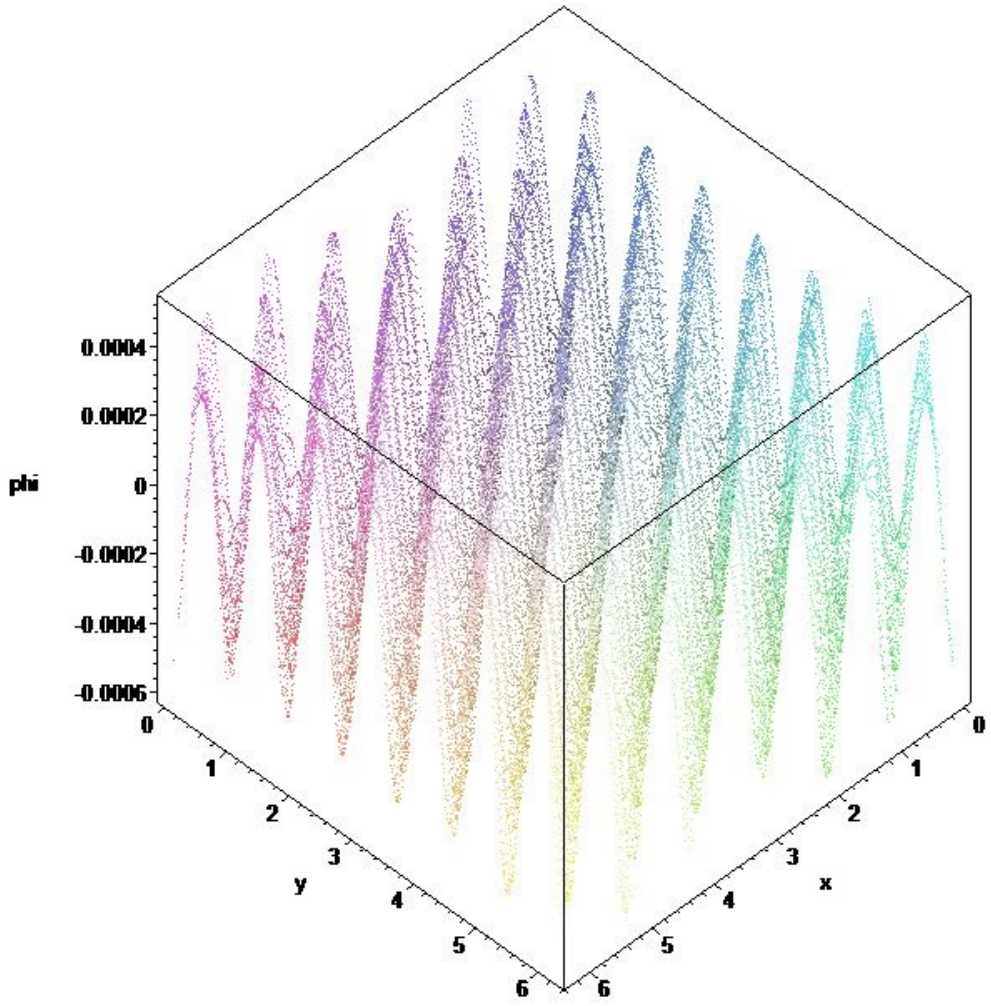

Figure 7.3: Difference between the latter half points of figures 7.1 and 7.2 of system (7.0.2) with parameter values (7.0.3)

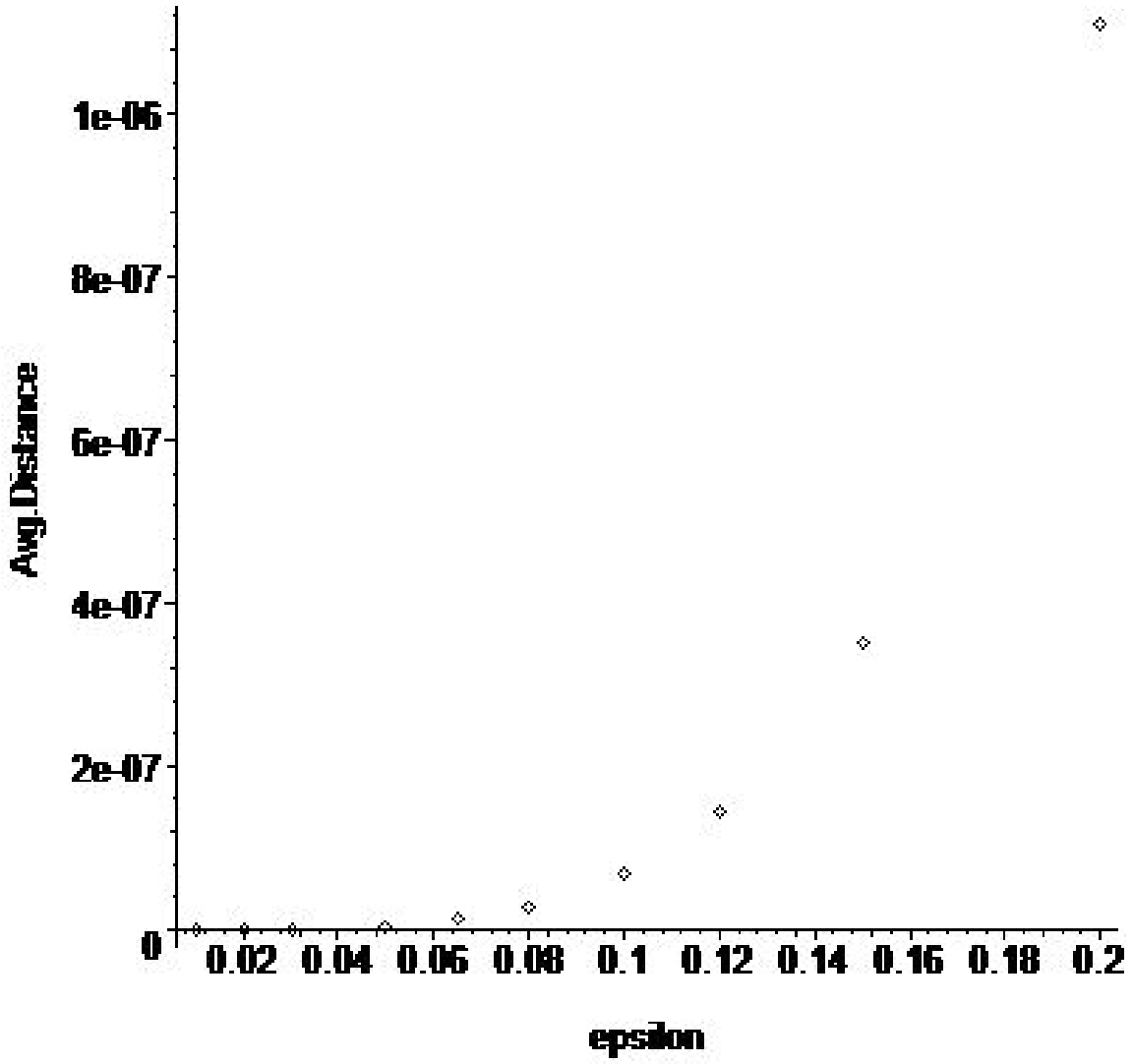

Figure 7.4: Average distance between the simulation and computed surface of system (7.0.2) for the latter half of 100 001 points.

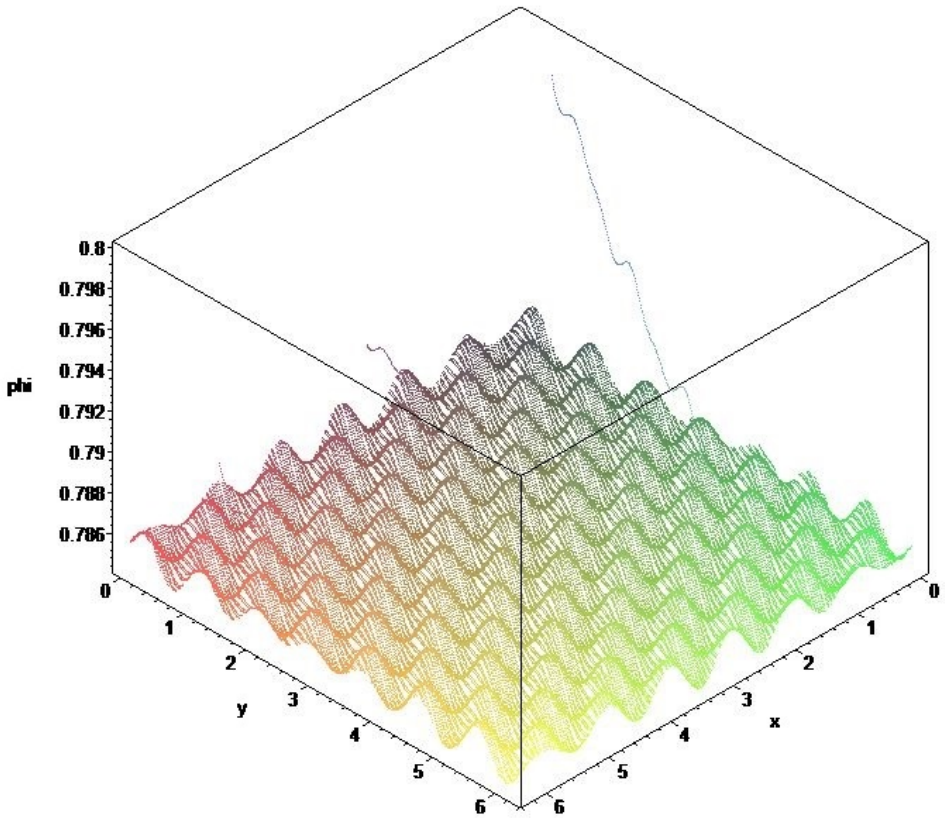

Figure 7.5: Simulation of a system which is exactly the same as (7.0.2), except for $\varphi(0) = 0.8$, and other parameter values (7.0.3).

Chapter 8

Conclusion

Spiral waves are an important phenomenon due to its occurence in many physical experiments and in physiological pathologies. In this thesis, we have analysed spiral waves in a medium with lattice symmetry using a dynamical system approach. The choice of such a perturbation was motivated by cellular patterns and gap junctions.

Going through the results we obtained, we can see that the effect of the lattice perturbation is not dissimilar to its symmetries. Indeed, after finding our general forms of the perturbation function, we investigated its effect on rigidly rotating waves. What we saw was that either the solution orbits a corner of the unit square and possess $\frac{\pi}{2}$ spatio-temporal symmetry or are part of a family of four obtained through such rotations. We also obtained some theoretical results on the stability of such orbits. The existence and symmetries of these orbits are shown with numerical examples and a Poincaré map approximation. For travelling waves, when $\omega = 0$, we used averaging methods and several changes of variables in order to prove the existence of invariant surfaces in the three-torus. This surface can be approximated with a Taylor expansion and the difference of the obtained approximation with numerical examples is usually on higher orders of ε. All these results are obtained using dynamical systems methods, which illustrates the importance of the center manifold reduction done in [8, 21].

However, the work presented in this thesis only manages to scratch the surface for the study of spiral waves under lattice perturbation. Many avenues may be considered in this subject in the future. One of which is to compare the results obtained here with solutions of the reaction-diffusion equation whence spiral waves came from. In fact some work by the author is currently in progress in this direction. One could gain further knowledge in this direction by finding the equivalences between the partial differential equation and the reduced ordinary equation, in this way going directly into dynamical systems from numerical or physical equations. One other obvious way to expand this research would be to include meandering in the equations. This requires the inclusion of the complex variable q into the equations. This way, one could even try to observe the resonant phenomenon where the solution goes into a linearly meandering trajectory, which is a principal area of interest in spiral wave research, as demonstrated in [13, 4] for example.

Appendix A

General Existence Theorem for Invariant Surfaces

In this appendix we state a theorem given in [9] which proves the existence of an invariant surface in some dynamical systems. To prove the existence of such a surface for the travelling wave in a lattice perturbation, we will need to adapt our equations in order to meet the assumption of this theorem.

Theorem A.0.1 (Theorem 2.3 in section VII.2 of [9]). *Consider the system*

$$\begin{aligned} \dot{\phi} &= \varepsilon A\phi + \varepsilon\Theta(X,\phi,\varepsilon) \\ \dot{X} &= \omega + \varepsilon F(X,\phi,\varepsilon), \end{aligned} \tag{A.0.1}$$

where $\phi \in \mathbb{R}^n$, $X \in \mathbb{R}^m$, $\omega \in \mathbb{R}^m$ is a constant vector, A is an n-by-n matrix of constants of block diagonal form

$$A = \begin{pmatrix} A_s & 0 \\ 0 & A_u \end{pmatrix},$$

where A_s has all eigenvalues with negative real part and A_u has all eigenvalues with positive real part. Define

$$\Omega(r_0,\varepsilon_0) = \{(x,\varepsilon) : |x| < r_0, 0 \le \varepsilon \le \varepsilon_0\}.$$

Suppose that F, Θ satisfy the following conditions:

(C1) F and Θ are continuous and bounded in $\mathbb{R}^m \times \Omega(r_0, \varepsilon_0)$.

(C2) F and Θ are Lipschitz in X in $\mathbb{R}^m \times \Omega(r_0, \varepsilon_0)$, with Lipschitz constants $L_X^F(r,\varepsilon)$ and $L_X^\Theta(r,\varepsilon)$ respectively, where $L_X^F(r,\varepsilon)$, $L_X^\Theta(r,\varepsilon)$ are continuous and nondecreasing for $0 \le r \le r_0$, $0 \le \varepsilon \le \varepsilon_0$, and $L_X^\Theta(0,0) = 0$.

(C3) F and Θ are Lipschitz in ϕ in $\mathbb{R}^m \times \Omega(r_0, \varepsilon_0)$, with Lipschitz constants $L_\phi^F(r,\varepsilon)$ and $L_\phi^\Theta(r,\varepsilon)$ respectively, where $L_\phi^F(r,\varepsilon)$, $L_\phi^\Theta(r,\varepsilon)$ are continuous and nondecreasing for $0 \le r \le r_0$, $0 \le \varepsilon \le \varepsilon_0$, and $L_\phi^\Theta(0,0) = 0$.

(C4) The function $|\Theta(X,0,\varepsilon)|$ is bounded by $N(\varepsilon)$ for $X \in \mathbb{R}^m$, $0 \le \varepsilon \le \varepsilon_0$, where $N(\varepsilon)$ is continuous and nondecreasing for $0 \le \varepsilon \le \varepsilon_0$, and $N(0) = 0$.

Furthermore, since the matrix A has all eigenvalues away from the imaginary axis, there exists $\alpha > 0$, $K > 0$ such that for any real number τ,

$$|e^{(t-\tau)\varepsilon A_s}| \le K e^{-\varepsilon\alpha(t-\tau)}, \quad t \ge \tau$$
$$|e^{(t-\tau)\varepsilon A_u}| \le K e^{-\varepsilon\alpha(t-\tau)}, \quad t \le \tau.$$

Suppose that $\alpha - \limsup_{\varepsilon\to 0} L_X^F(0,\varepsilon) > 0$.

Then the following conclusions are true for the system (A.0.1): There exist $\varepsilon_1 > 0$ and continuous functions $D(\varepsilon)$, $\Delta(\varepsilon)$, $0 < \varepsilon \le \varepsilon_1$, which approach zero as $\varepsilon \to 0$, and a continuous function

$$\sigma : \mathbb{R}^m \times (0, \varepsilon_1] \mapsto \mathbb{R}^n,$$

with $\sigma(X,\varepsilon)$ bounded by $D(\varepsilon)$, Lipschitz in X with Lipschitz constant $\Delta(\varepsilon)$, such that the set

$$S_\varepsilon = \{(X,\phi) : \phi = \sigma(X,\varepsilon), X \in \mathbb{R}^m\}$$

is an invariant set for the system (A.0.1). If the functions F and Θ in (A.0.1) are multiply periodic in X with period vector $(T_1, \cdots, T_m)$, then $\sigma(X,\varepsilon)$ is also multiply

periodic in X with period vector $(T_1, \cdots, T_m)$. Finally, the asymptotic stability of the invariant set S_ε is the same as that of the trivial equilibrium point of the equation $\dot{Y} = AY$.

In our system, we have $n = 1$ and $m = 2$, thus A becomes a real constant and the suppositions on K and α become trivial. If we were to summarize this in one sentence, the theorem states that if a system of ordinary equations (A.0.1) satisfies the conditions (C1) to (C4), then the limit sets of the solution for ϕ can be written as the range of a function of X and ε only. This set becomes more and more flat as ε goes to zero and its stability depends only on the eigenvalues of A (more specifically its sign in our $n = 1$ case). Since all the terms in our proof arise either from a Taylor series or the solution of a simple partial differential equation, we will assume that our perturbation terms are Lipschitz and continuous enough for our purposes. However we cannot assume that the Lipschitz constants go to zero as $\varepsilon \to 0$. Therefore we will need to adjust our system through near identity change of variables and averaging in order to make our system compatible to the form (A.0.1).

Bibliography

[1] V.1. Arnold. *Geometrical Methods in the Theory of Ordinary Differential Equations*. Springer, New York, 1988.

[2] D. Barkley. A model for fast computer simulation of waves in excitable media. *Physica D*, 49:61–70, 1991.

[3] D. Barkley. Linear stability analysis of rotating waves in excitable media. *Physical Review Letters*, 68(13):2090–2093, Mar 1992.

[4] D. Barkley. Euclidian symmetry and the dynamics of rotating spiral waves. *Physical Review Letters*, 72(1):164–167, Jan 1994.

[5] P. Boily, V. G. LeBlanc, and E. Matsui. Spiral anchoring in media with multiple inhomogeneities: A dynamical system approach. *Journal of Nonlinear Science*, 17:399–427, 2007.

[6] Paul C Bressloff, Jack D Cowan, Martin Golubitsky, Peter J Thomas, and Matthew C Wiener. Geometric visual hallucinations, euclidean symmetry and the functional architecture of striate cortex. *Philosophical Transactions of the Royal Society of London. Series B: Biological Sciences*, 356(1407):299–330, 2001.

[7] M Georgi and N Jangle. Spiral wave motion in reaction-diffusion systems. In *Equadiff 2003: International Conference On Differential Equations*, pages 651–

656, SINGAPORE, 2005. World Scientific Publ Co Pte Ltd. International Conference on Differential Equations, Hasselt, Belgium, Jul 22-26, 2003.

[8] M. Golubitsky, V. G. LeBlanc, and I. I. Melbourne. Meandering of the spiral tip: An alternative approach. *Journal of Nonlinear Science*, 7:557–586, 1997.

[9] J. K. Hale. *Ordinary Differential Equations, 2nd Edition.* Robert E. Krieger Publishing Company, Florida, 1980.

[10] E. Hecht. *Optique.* Pearson Education France, Paris, 2005.

[11] J.P. Keener and J. Sneyd. *Mathematical Physiology.* Interdisciplinary applied mathematics: Mathematical biology. Springer Verlag, 1998.

[12] Jeroen S.W. Lamb and Claudia Wulff. Pinning and locking of discrete waves. *Physics Letters A*, 267(23):167 – 173, 2000.

[13] V. G. LeBlanc. Rotational symmetry breaking for spiral waves. *Nonlinearity*, 15:1179–1203, 2002.

[14] V. G. LeBlanc and B. J. Roth. Meandering of spiral waves in anisotropic tissue. *Dynamics of Continuous, Discrete and Impulsive Systems Series B: Applications & Algorithms*, 10:29–41, 2003.

[15] V. G. LeBlanc and C. Wulff. Translational symmetry-breaking for spiral waves. *Journal of Nonlinear Science*, 10:569–601, 2000.

[16] Alberto P. Muñuzuri, Vicente Pérez-Muñuzuri, and Vicente Pérez-Villar. Attraction and repulsion of spiral waves by localized inhomogeneities in excitable media. *Phys. Rev. E*, 58:R2689–R2692, Sep 1998.

[17] B. J. Roth. Frequency locking of meandering spiral waves in cardiac tissue. *Phys. Rev. E*, 57:R3735–R3738, 1998.

[18] B. J. Roth. Meandering of spiral waves in anisotropic cardiac tissue. *Physica D*, 150:127–136, 2007.

[19] J.A. Sanders, F. Verhulst, and J. Murdock. *Averaging Methods in Nonlinear Dynamical Systems*. Applied Mathematical Sciences. Springer, 2007.

[20] B. Sandstede, A. Scheel, and C. Wulff. Center-manifold reduction for spiral waves. *Comptes Rendus de l'Académie des Sciences*, 324(I):153–158, 1997.

[21] B. Sandstede, A. Scheel, and C. Wulff. Dynamics of spiral waves on unbounded domains using center-manifold reductions. *Journal of Differential Equations*, 141:122–149, 1997.

[22] A. T. Winfree. Scroll-shaped waves of chemical activity in three dimensions. *Science*, 181(4103):937–939, Sep 1973.

[23] V. S. Zykov and S. C. Müller. Spiral waves on circular and spherical domains of excitable medium. *Physica D*, 97:322–332, 1996.